The Reduction of Supersonic Jet Noise Using
Pulsed Microjet Injection

by

Paul Aaron Ragaller

B.S. Mechanical Engineering
Case Western Reserve University, 2005

Submitted to the Department of Mechanical Engineering
in Partial Fulfillment of the Requirements for the Degree of
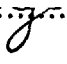
Master of Science in Mechanical Engineering

at the

Massachusetts Institute of Technology

September 2007

Signature of Author...
Department of Mechanical Engineering
August 22, 2007

Certified by...
Anuradha Annaswamy
Senior Research Scientist
Thesis Supervisor

Accepted by...
Lallit Anand
Chairman, Committee for Graduate Students
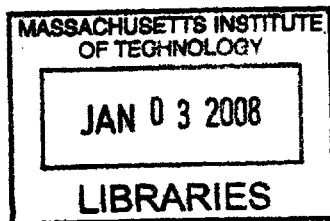
The Reduction of Supersonic Jet Noise Using
Pulsed Microjet Injection

by

Paul Aaron Ragaller

Submitted to the Department of Mechanical Engineering
on August 25, 2007 in Partial Fulfillment of the
Requirements for the Degree of Master of Science in
Mechanical Engineering

ABSTRACT

This thesis is concerned with the active control of supersonic jet noise using pulsed microjet injection at the nozzle exit. Experimental investigations were carried out using this control method on an ideally expanded Mach 1.8 jet operating at 900, 1300 and 1700°F. Six Bosch fuel injectors were modified and mounted on a toroidal manifold around a Mach 1.8 nozzle. Noise data were collected from the jet at baseline condition, which refers to the uncontrolled case. The injectors were fired at pressures of 400 and 800 psig, using water, at frequencies of 1, 5 and 10 Hz and at duty cycles of 50 and 75%. For comparison, acoustic data were also collected from the jet while the microjets were injecting steadily at a constant pressure.

The results led to the following two conclusions: for injection at a given mass flow rate, noise reductions are higher with pulsed injection compared to the steady case, and for injection at a given pressure, the amount of noise reduction increases with duty cycle. In particular, for pulsing at a 50% duty cycle, pulsing achieves comparable noise reduction as compared to steady injection at all of the temperatures tested while using only 66% of the mass flow rate. The most dramatic result was achieved at 1700°F for pulsing at a 75% duty cycle with an injection pressure of 800 psig. In this case, pulsing achieves 317% of the noise reduction as compared to steady injection (corresponding to 2.6 and 0.8 dB respectively) while using a comparable amount of water. Similar results were obtained at lower temperatures as well. At all operating points it was found that less water is used with pulsing to achieve a given noise reduction, and is realized at the cost of a higher injection pressure. Suggestions are provided as to how to determine the frequency and duty cycle required for maximum noise suppression with the least amount of water.

Thesis Supervisor: Anuradha Annaswamy
Title: Senior Research Scientist

3

ACKNOWLEDGEMENTS

First and foremost, I would like to thank Dr. Anuradha Annaswamy, my thesis advisor, for her guidance, support, enthusiasm and attention to detail. With her leadership I have changed my way of thinking and have learned to see the bigger picture.

None of the work presented here would have been possible without the generous funding provided by our contacts at Boeing – namely, Krishnan Viswanathan and his group. Their support and confidence is greatly appreciated.

The work performed at Florida State University would never have been possible without the help of several people. I would like to thank Dr. Anjaneyulu Krothapalli for his expertise, enthusiasm and dedication to this project. I would also like to extend a special thanks to Dr. Brenton Greska for allowing me to absorb as much knowledge about jet noise, the facility and experimentation in general as possible during my time in the facility. Special mention goes to Bobby Avant, the lab machinist, who made many of the facility adaptations possible.

Special mention goes to Sungbae Park and the Robert Bosch Corporation for providing us with eight fuel injectors and a special driver to run them all. They took time to understand our situation and deliver us the best products for the job. Without their help, I would still be looking for the perfect injector.

Thanks to my mother, Carol, for lending her support and her occasional reminders that deadlines are closer than they appear. Thanks to my father, Bill, for his encouragement and reinforcement. Thanks to Alvin for being such a great friend. Thanks to Noah for being so proud of me.

The help and consideration of those mentioned above is sincerely appreciated.

TABLE OF CONTENTS

LIST OF FIGURES

9

10

CHAPTER 1

INTRODUCTION AND BACKGROUND

As passenger and military aircraft become larger, faster and more powerful, the noise generated by their engines becomes louder. In the commercial setting, most aircraft travel subsonically. Their engines are of the high-bypass, turbofan variety, which consist of two parts. At the center is a powerful gas turbine. Air enters the turbine and is compressed by the many rows of blades, then mixes with fuel. The fuel-air mixture combusts in the center of the turbine, then exits at high velocity through another set of blades. The combusted, high-speed air is exhausted through a relatively small nozzle. Meanwhile, ambient air is dawn around the outside of this turbine by a large fan. The mass of air drawn around the turbine is sometimes three times more than the air drawn into the turbine itself—hence the term "high-bypass". As such, a large amount of fluid is accelerated by only a small amount. Originally designed to provide more thrust, the co-flow exhaust of these engines also helps to reduce the noise generated—an unintended advantage. The noise pollution caused by such aircraft during takeoff, landing and run-up time (the time the aircraft spends idle or taxiing with the engines on), however, becomes a serious issue with regards to neighborhoods that surround and encroach upon airports. This drives property values down and poses a general annoyance to those citizens living nearby. Military aircraft are generally supersonic and are powered by turbojet engines. These engines are similar to those used on commercial aircraft but with different inlet geometry which decelerates the fluid to subsonic speeds, thus abating the harmful effects of shock waves. The high-pressure, high-temperature exhaust then passes through a converging-diverging nozzle, which accelerates the fluid to supersonic speeds. The balance of momentum across the engine produces a large amount of thrust. Though

military aircraft rarely operate near residential areas and pose little annoyance to the general public, they do operate frequently within the confines of military vessels, such as aircraft carriers. Such carriers require on-deck labor—this means that someone must stand on deck and guide these aircraft during run-up and takeoff. However, the development of equipment designed to protect these deckhands against the harmful effects of high-intensity noise generated by these aircraft has not kept up with the development of faster, more powerful engines. This leaves these individuals exposed to harmful noise radiation. Therefore, any method or device designed to reduce the noise generated by an aircraft, without also reducing thrust, would prove advantageous on all fronts of this issue.

The greatest public misconception regarding the source of jet noise is the belief that the majority of the noise is generated within the engine itself. While it is true that some noise is produced by the combustion process and from moving and vibrating parts within the engine, this noise does not contribute significantly to the overall noise production of the jet engine. Interestingly, the majority of the noise is generated aft of the nozzle exit. There are two main processes that contribute substantially to the generation of jet noise—though understanding them requires a small amount of background knowledge of the structure of a free jet.

In practice, as well as in experimentation, high-speed fluid generated within the jet engine exhausts to open atmosphere. Whether this open atmosphere is quiescent, as in the laboratory setting, or moving, as with an aircraft, it generally appears to be moving with a much lower velocity with respect to the jet exhaust. Therefore, the jet of high-speed exhaust fluid is forced to interact with the ambient fluid. Figure 1.1 is a simple schematic of a high-speed jet issuing into ambient fluid.

Potential Core **Shear Layer** **Sonic Line**

Potential Core Region | **Transition Region** | **Fully Developed Region**
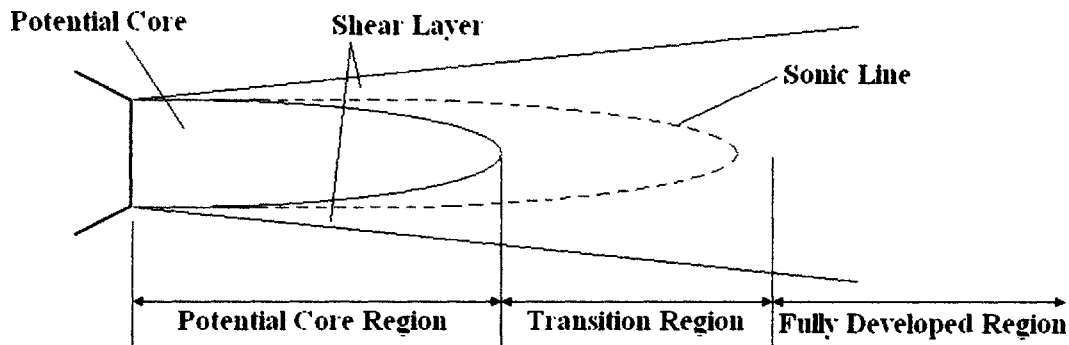
Figure 1.1: Simple schematic of the development of a high-speed jet as it issues into the ambient medium.

As the jet issues into the ambient medium, viscous forces cause velocity gradients to form at the boundary of the jet, which in turn causes the two fluids to mix. The region where these gradients and mixing occur is known as the shear layer. Moving downstream, the thickness of the shear layer grows and intrudes on the potential core. The potential core is the region of the jet where the axial velocity is at least 99% of the velocity of the fluid exiting the nozzle. Eventually, the shear layers meet in the middle and the potential core ends. This is the beginning of the transition region. Even farther downstream, the velocity profiles become self-similar and the jet is in its fully developed region. The growth rate of the shear layer, and thus the length of the potential core, varies depending on the running conditions of the jet. Also pictured in Figure 1.1 is the sonic line. Inside the sonic line, the fluid is moving faster than the speed of sound relative to the ambient medium.

High-Speed Side

Shear Layer

Ambient fluid
entrained

Low-Speed Side
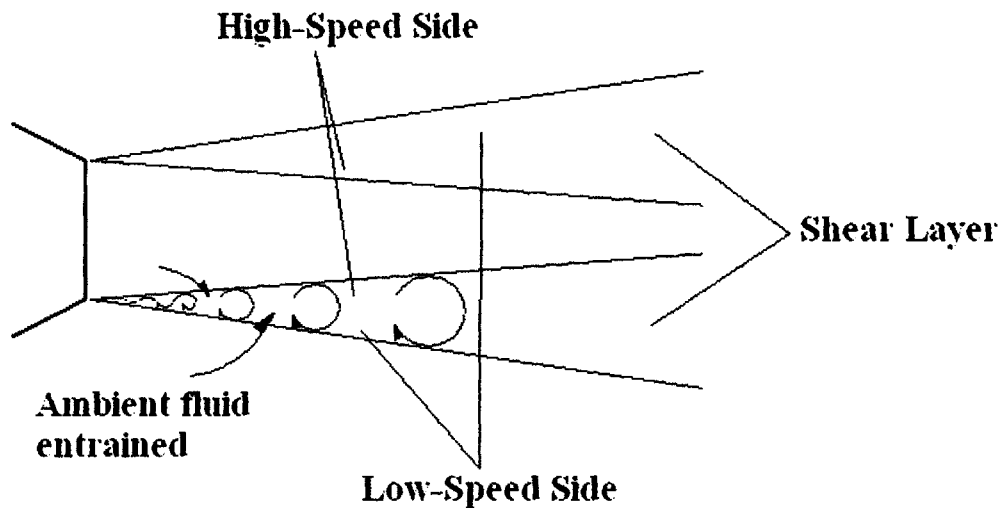
Figure 1.2: Simple illustration of the inception and growth of large, coherent structures, and the entrainment of fluid within.

As stated before, the growth rate of the shear layer depends entirely on the properties of the jet. However, Papamoschou and Roshko were some of the first to discover that the shear layer of a supersonic jet grows more slowly than that of a subsonic jet [1]. This lends itself to the fact that supersonic jets have longer potential cores than their subsonic counterparts. The potential core itself is a large source of broadband mixing noise. Aside from this, Crow and Champagne found that velocity gradients were responsible for producing coherent structures with high vorticity [2]. These structures propagate downstream at velocities greater than the speed of sound with respect to the ambient medium. Moore found that these eddies are formed from initial instability waves and grow as they travel downstream [3]. He also found that these eddies entrain ambient fluid and can interact with each other, thus enhancing mixing in the shear layer. Figure 1.2 is a simple illustration of this concept. This figure also shows a light line roughly delineating the low-speed and high-speed sides of the shear layer. These coherent structures were found by Bishop, Ffowcs Williams and Smith to be responsible for Mach wave radiation, another significant noise source in a supersonic jet [4]. Figure 1.3 shows a simple schematic of the growth of these eddies with respect to Mach wave radiation. Bishop, Ffowcs Williams and Smith also noted that the Mach waves tended to favor the high-speed side of the shear layer [4]. Thus, the Mach waves seem to be born from the extreme pressure gradients at the leading edge of each eddy. Therefore, as in Figure 1.3, the Mach waves are formed and propagate from the leading edge of the structure.

14
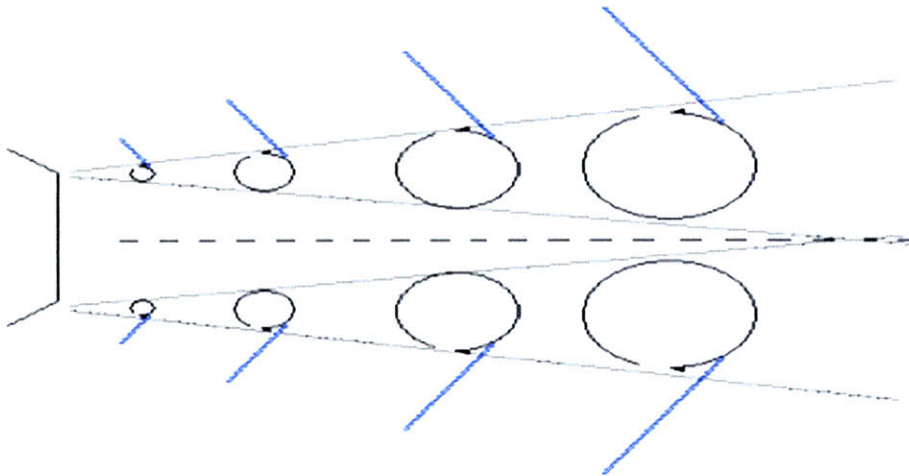
Figure 1.3: Schematic of the simultaneous growth and propagation of coherent eddies and Mach wave radiation.

Aside from mixing noise and Mach wave radiation, screeching also contributes significantly to supersonic jet noise. Screeching, however, is generally only present when the jet is operated with an off-design condition. Screech tones occur at discrete frequencies, and were first identified by Powell [5]. Small disturbances are generated as the shock cells generated as a result of the off-design run condition interact with the shear layer. These disturbances travel upstream and reflect off of the nozzle lip. They then travel back to their originating position and interfere constructively with newly generated disturbances. This process of feedback continues until a screech tone is generated. Screeching proves to be a larger problem than simple tones: Alkislar showed that screeching can cause heightened Mach wave radiation [6]. Screech tones are easily quelled, however, by simply breaking the feedback loop. This can be done by decreasing the thickness of the nozzle lip or through the use of an external control such as microjet injection.
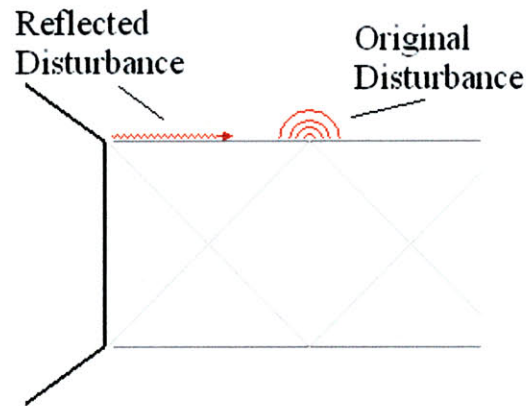
Figure 1.4: Schematic of the screech tone generation mechanism.

There have been several attempts to reduce the noise generated by a jet, though most come with large disadvantages. Many studies have focused on the use of chevrons and tabs. These consist of tabs of material that protrude from the nozzle into the jet exhaust. Bradbury and Khadem as well as Samimy, Zaman and Reeder showed that significant noise reduction could be achieved using tabs [7, 8]. However, this comes with one stark disadvantage: the tabs present themselves as a source of drag, thus producing an unacceptable amount of thrust loss. Also, tabs and chevrons cause an energy shift in the frequency spectrum. While the noise generated at low frequencies is decreased, high-frequency noise is increased. Therefore, the reductions presented occur only in certain directions. Papamoschou developed a co-flow technique for supersonic jets similar to the high-bypass engines used on commercial, subsonic aircraft [9, 10]. While this was effective in reducing the overall noise, the inlet area required was too large to allow for its practical use. Raman, Kibens, Cain and Lepicovsky developed a technique involving a high-speed actuator [11]. The actuator would introduce tones into the exhaust to control the characteristics of the fluid flow. However, the reductions produced were marginal at best.

Much work has been done involving a new technique of jet noise suppression. Performed by Greska, this technique involves control by means of fluidic microjet injection [12]. Several small nozzles are positioned at the nozzle exit pointing into the flow. These nozzles may inject any medium, which penetrates the shear layer of the jet. This sets up streamwise vortices that inhibit the formation and growth of large-scale structures and eddies. This effect was shown by Alkislar, Krothapalli and Butler [13].

16

This technique is able to achieve large noise reductions (up to 8 dB). Since the microjet nozzles themselves do not interfere with the flow of the main jet, no drag is produced. If anything, a small, yet probably negligible, amount of thrust is generated as a result of the momentum balance across the nozzles. The work in this thesis concerns itself with this technique of jet noise suppression.

The main disadvantage of using microjet injection for noise suppression is the fact that the best reductions are achieved with water as the injection medium. With a density of about 1000 kg/m^3, water is a heavy fluid to carry onboard an aircraft. Therefore, if the amount of water used could be reduced without compromising the noise reduction of the jet, this method would prove superior. One way to reduce the amount of water used is to pulse the microjet injection—thereby reducing the amount of water used based on the parameters of the pulsing. This thesis will investigate the ability of pulsed microjet injection to reduce the noise of a supersonic jet while using less water than the steady microjet injection performed by Greska [12].

CHAPTER 2

EXPERIMENTAL SETUP

2.1 Overview

This investigation involves a set of experiments that required a high-temperature, high-pressure, supersonic jet facility. Therefore, they were carried out at the High Temperature Supersonic Jet Facility, which is located at the Fluid Mechanics Research Laboratory on the Florida State University main campus. The facility consists of three adjacent rooms and a high-pressure air supply. The air supply enters the first of the three rooms, dubbed the burner room, where it is reduced to a desired pressure. The air then enters a sudden expansion (SUE) burner where combustion occurs. The high-pressure, high-temperature airflow is then exhausted to the second room—a fully anechoic chamber—where it interacts with the ambient environment then exits to the atmosphere via an acoustically treated exhaust duct. Acoustic and ambient measurements are made in the anechoic chamber. All of the jet parameters are controlled and monitored from the third room—the control room. An overall schematic of the facility is shown in Figure 2.1.1. While a brief description of the facility is presented here, a more in-depth discussion can be found in Greska [12].
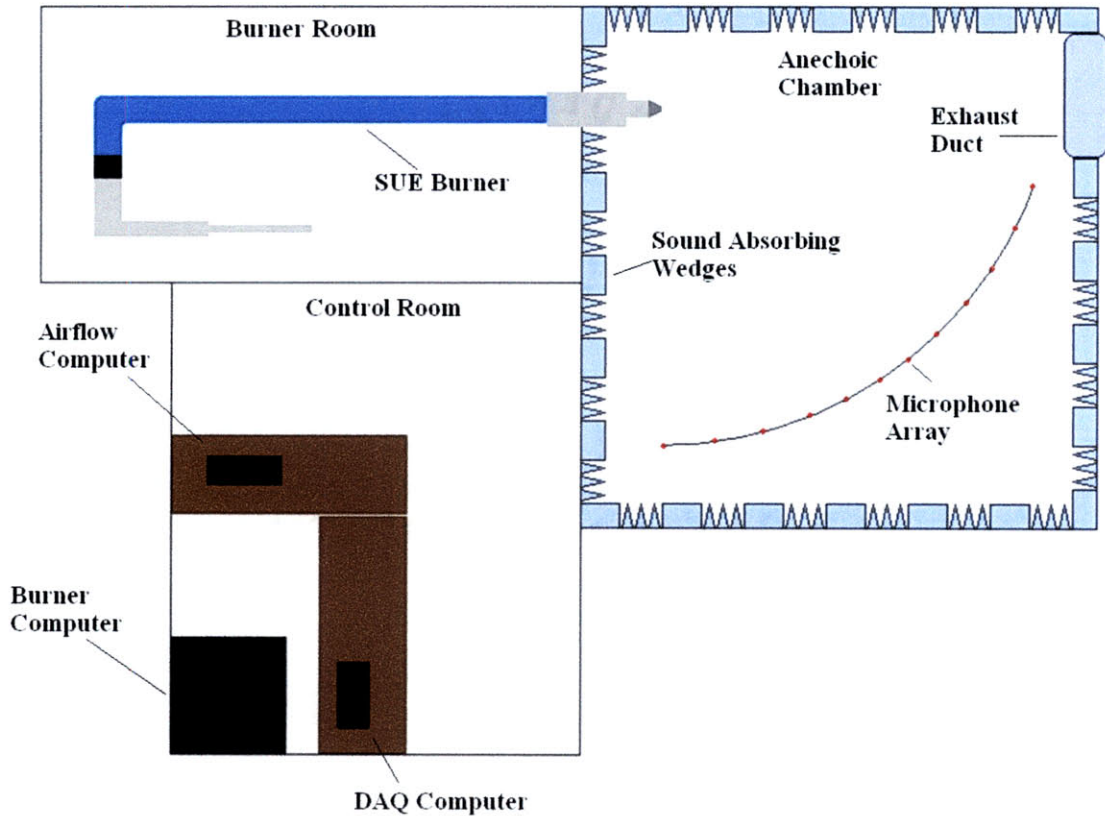
Figure 2.1.1: Simple schematic of the high-temperature, supersonic jet facility.

2.2 High Pressure Air Supply

Air is pressurized by means of a CompAir MAKO model 5436-60E3, four-stage, high-displacement, reciprocating air compressor. This compressor has an output of 80 CFM. The local air in Tallahassee, Florida tends to be very humid, and any moisture in the air will condense within the facility, so the compressed air is then dried using a Zander model HPRDF200-W refrigerated air dryer. Oil and particulates from the atmosphere and compressor are removed by a series of filters through which the compressed air passes after leaving the refrigerators. These particulates, if not removed, would decrease the performance of the pressure regulating equipment within the facility.

The pressurized and cleaned air is then stored in a series of four interconnected storage tanks. The first of which has a volume of 5 m^3, while the remaining three (which are identical) have a combined volume of 5 m^3 giving a total storage capacity of 10 m^3. Air in the tanks is pressurized to 2000 psig, and the experiments can be run until the pressure is depleted to about 500 psig. This capacity allows for a run time between 20 and 45 minutes, depending on the jet operating conditions. It takes about eight hours for

the pressure in the tanks to be fully replenished. Figure 2.2.1 shows a schematic of the high-pressure air supply system.
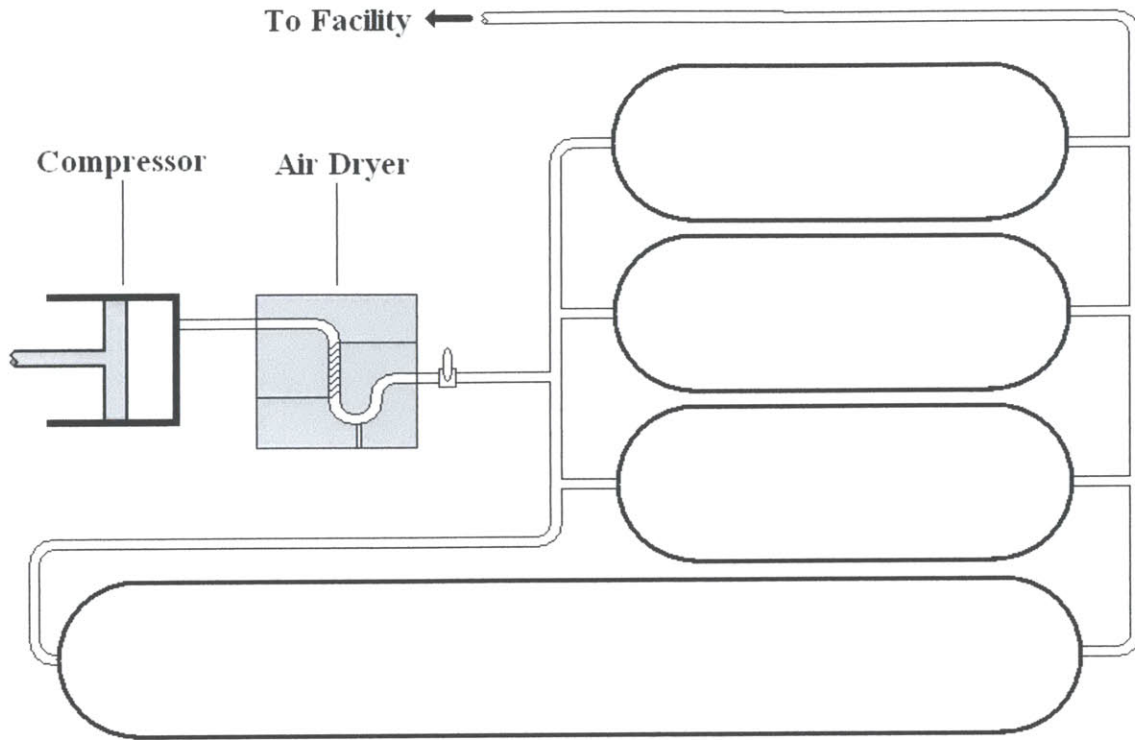
Figure 2.2.1: Simple schematic of the air supply system.

2.3 Burner Room

The high-pressure air is routed into the burner room via a network of 1.25-inch schedule 160 piping. In the burner room, the air first passes through a Jamesbury model SP200-B double-acting solenoid shut-off valve. It then passes through a 2.5-inch schedule 80 pipe on its way to the two-stage pressure control system. This consists of two 2-inch Leslie Aeroflow high-performance control valves. The first valve is designed to have a large pressure drop so that the pressure can be reduced from supply to 300 psig if necessary. The second valve has a low-pressure drop, and is used mainly for fine adjustments to the pressure. After each of the valves, for safety reasons, a Hydroseal relief valve is implemented. The upstream relief valve is set to 1100 psig while the downstream relief valve is set to 300 psig.

To ensure that the flow does not reach sonic condition where the air mass flow measurements are made, especially when nozzles with larger throat diameters are used, a new venturi was designed and installed. The former venturi employed a 1.2-inch

diameter throat to measure the static pressure. A flat plate surrounding the mouth of the venturi held the stagnation pressure probe. The new venturi features a super-ellipse profile that keeps the flow from separating as it enters the test section. This super-ellipse is defined by:

$$h(x) = b\sqrt{1 - \left(\frac{a-x}{a}\right)^{2+(x/a)^2}} \; .$$

Both static and dynamic pressure measurements are made in the same plane within the test section of the venturi. This section has an inside diameter of 2.25 inches—larger than the largest throat diameter of any of the jet nozzles used. Figure 2.3.1 shows the profile of the venturi. Since the venturi is physically located before the SUE burner, we can guarantee that the flow does not become sonic therein. A mirror of the same super-ellipse is used to blend the measurement section into a 6° sloped section. This section brings the diameter back to the original pipe diameter. The total length of the venturi is eight inches.
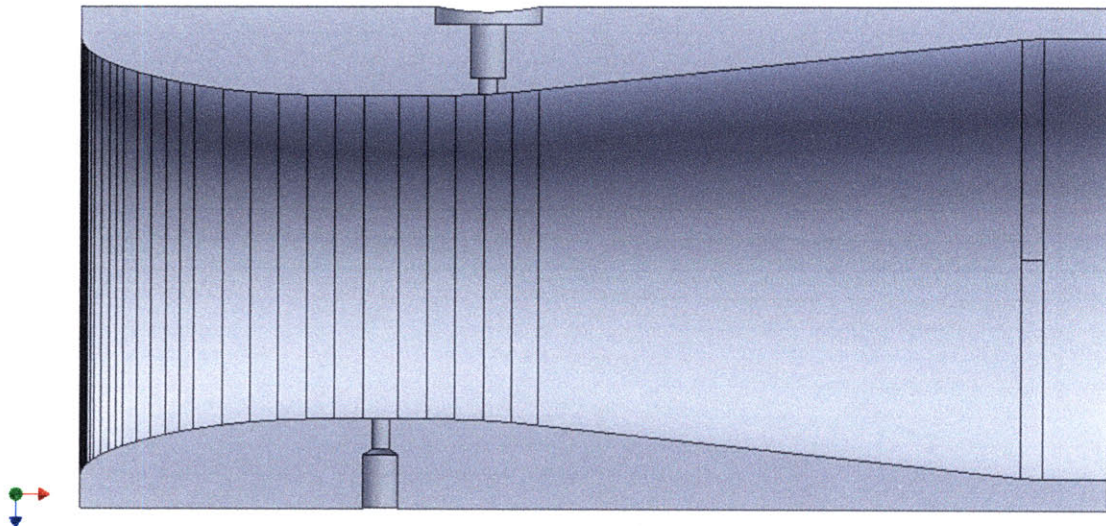
Figure 2.3.1: Cross section of the venturi. Holes are drilled for the static and dynamic pressure taps.

The pressurized air then enters the SUE burner. While most hot jet facilities use electric heaters, those that use combustion burn propane (which tends to limit the maximum stagnation temperature to 1100 K). This facility uses ethylene as the fuel; its combustion can produce flows with stagnation temperatures up to 1700 K, and enables run conditions that simulate realistic jet conditions. A standard automotive spark plug is

used to initially ignite the ethylene, which is fed in initially through a single tube. Six tubes inject gaseous ethylene fuel (which is fed from eight bottles in a closed, outward-facing compartment of the burner room) into the stagnation region of the expansion, thus guaranteeing a rich fuel/air mixture. The combustion of this mixture produces a high-temperature, high-pressure flow. After passing through a 1-inch thick ceramic flow straightener, the flow passes through a section where temperature and pressure are measured. Four equally spaced holes are drilled radially in this section, and an extrusion on each hole allows for the use of ¼-inch male NPT fittings. Into two opposing holes are inserted C-type thermocouples that measure the temperature of the flow. The stagnation pressure is measured via the other two holes. Since the flow is relatively slow in this section, the stagnation and static pressures are nearly equal. The flow then travels through another straight section, then a reducing section, then finally through an adapter. The nozzles are attached directly to this adapter. Each section is attached to the previous section with flanges and custom made Flexitallic Inconel gaskets, which prevent leaks at the joints.

2.4 Nozzles

Five nozzles were fabricated to allow for different operating conditions. Four converging-diverging (C-D), axisymmetric nozzles were made to allow for supersonic flows at Mach numbers of 1.3, 1.5, 1.8 and 2.0. A fifth nozzle with a converging (C), axisymmetric profile was made to provide subsonic and sonic flows at Mach numbers of 1.0 and below. Examples of both C-D and C nozzle profiles are given in Figure 2.4.1. The lip at the exit of each nozzle was kept as small as possible to minimize jet screeching. Larger lips allow for disturbances, which are reflected by large-scale structures, to reflect and amplify into tones. This enhances the overall broadband noise. While microjets easily quell this feedback loop, the baseline conditions without microjets will produce more noise, which will cause inaccurate baseline measurements. The lip of each nozzle was kept less than 1 mm. All of the experiments contained within this thesis, unless specifically stated, were performed using the Mach 1.8 nozzle at the ideally expanded operating condition.

23
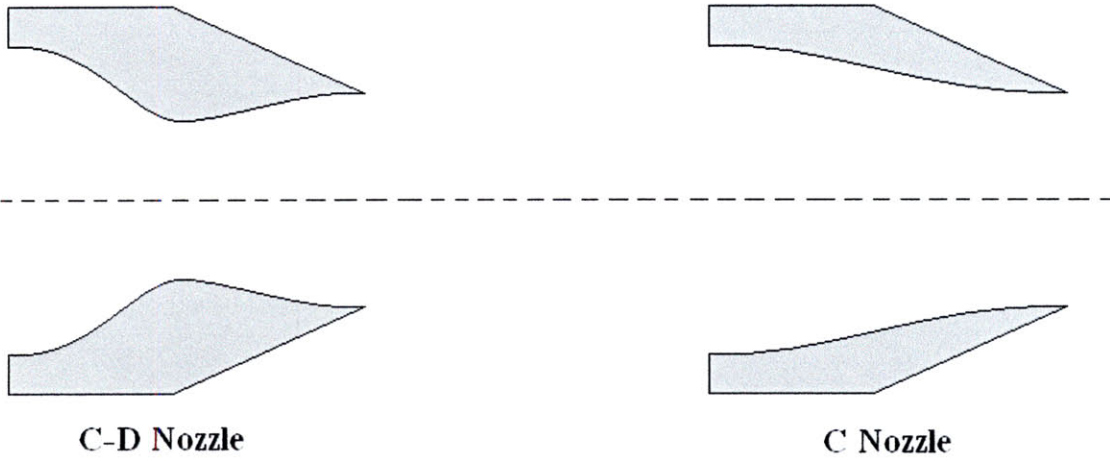
C-D Nozzle   **C Nozzle**

Figure 2.4.1: Nozzle types. On the left is a converging-diverging (C-D) nozzle used for supersonic flow generation. On the right is a converging (C) nozzle used for subsonic and sonic flow.
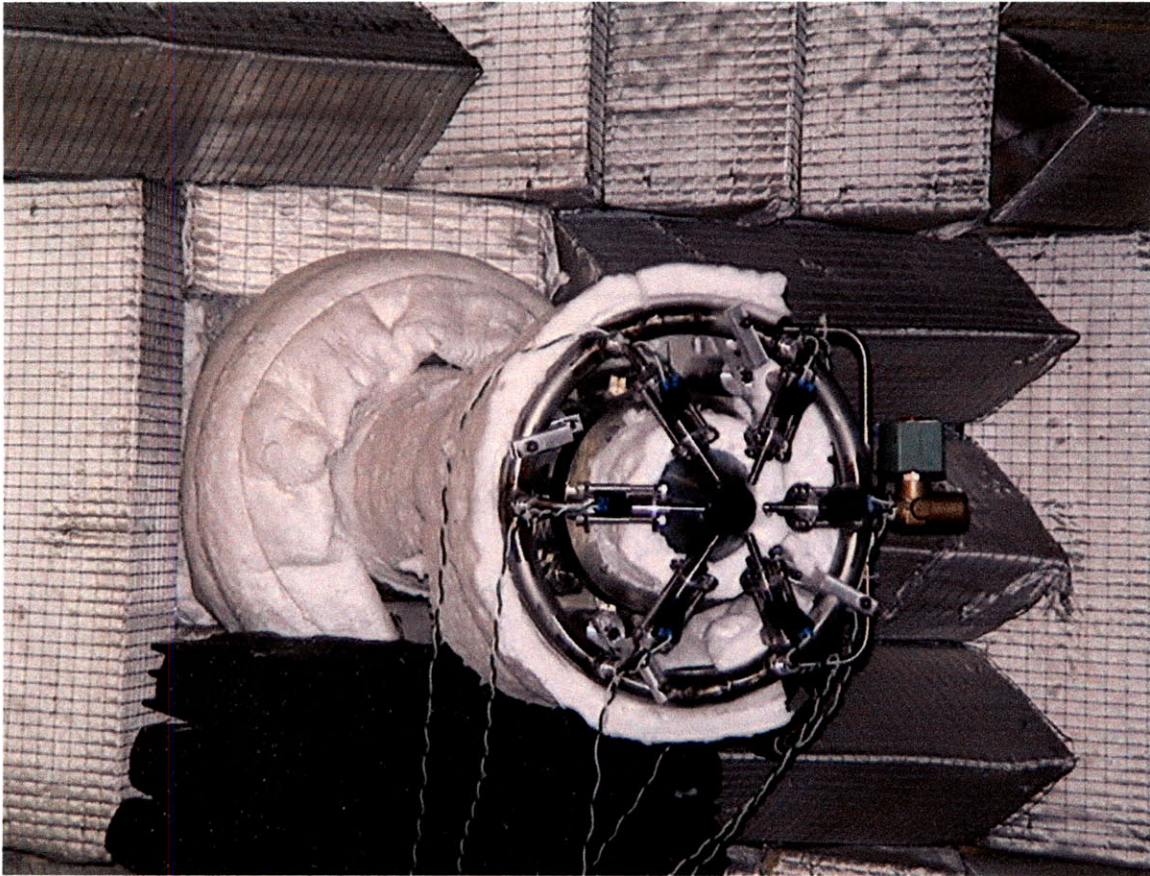
Figure 2.5.1: Six injectors are mounted around the nozzle. They are fed from the toroidal manifold.

2.5 Pulsed Microjet Injection

Nitrogen is used to pressurize the microjets. Three nitrogen tanks are used as the high-pressure store, and they feed into a dome regulator. This dome regulator, a Tescom model 26-1121-262, is located in the burner room with the tanks and controlled from the control room. This allows the pressure to be set and changed from a remote location so that no one has to enter the burner room while experiments are in progress.

The microjets can be run with either water or nitrogen as the injection medium. When nitrogen is used, the supply gas is passed through 3/8-inch stainless steel tubing to a Brooks model 3853i flow meter located in the burner room. The same tubing then takes the gas into the anechoic chamber where it reaches a toroidal manifold. The pressure of the fluid is monitored in the manifold via four pressure taps that are evenly spaced around the backside of the ring. Six 3/8-inch Swagelok fittings were fish-mouthed and welded to the front side of the ring manifold at evenly spaced locations. Six feeder tubes connect the microjets to the manifold and hold them at an angle of 60° to the jet axis. Figure 2.5.1 shows the microjets mounted on the manifold around the nozzle. When water is used, a separate tank is employed. Air at the desired pressure enters the tank and forces the water up a long tube that extends down to the bottom of the tank. The water travels through the same 3/8-inch tubing out to the circular manifold. When water is injected the flow meter is not used as it is calibrated with nitrogen as the working fluid. Water flow rates are determined experimentally with an individual microjet. A schematic of the injection system is shown in Figure 2.5.2.
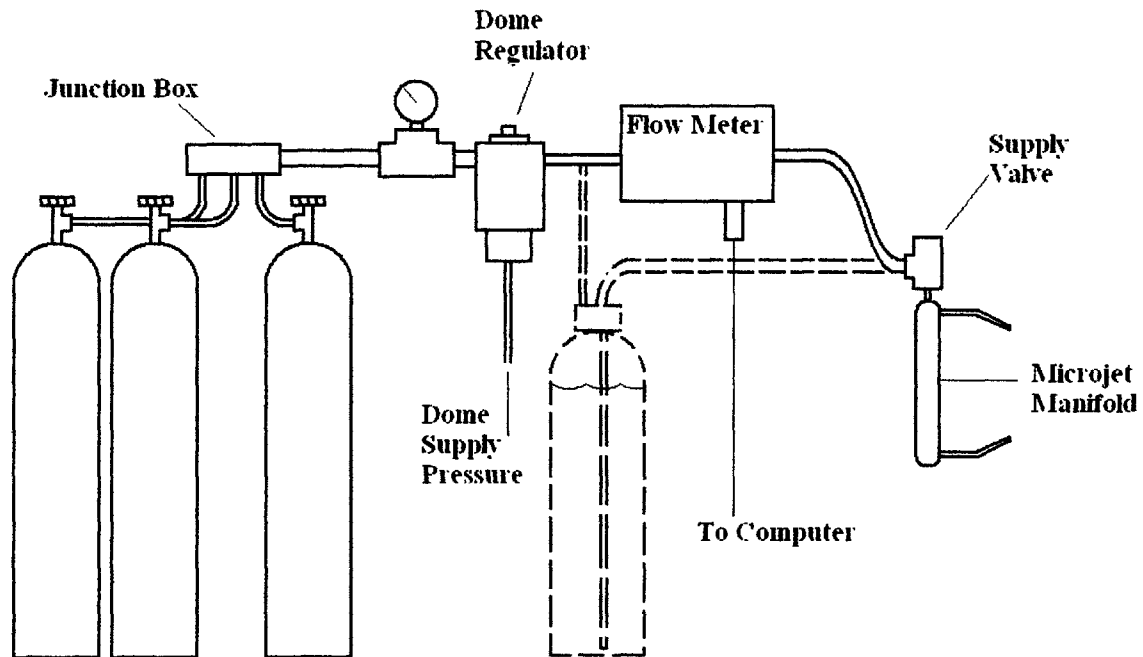
Figure 2.5.2: Simple schematic of the microjet injection system.

Each microjet consists of a modified Bosch HDEV-1 Fuel injector (06F 906 036 A). Out of the box, the injectors are equipped with an atomizer tip. In a diesel automobile engine, mixing is desired between the fuel and air inside the cylinder. To accomplish this, atomizers are built into the injector to ensure a fine particulate mist is emitted into the cylinder. For our application, a concentrated jet is desired. Therefore, the atomizer tip was cut off and new tips were machined and installed. These tips mimic the design of the original tip, but they produce a concentrated jet of fluid. A drawing of the new tip is shown in Figure 2.5.3. Fluid flows around the plunger and through holes bored into the side of the tip. There, the fluid is either inhibited by the plunger (while closed) or allowed to flow through the exit (while actuated). An exploded view of these parts is shown in Figure 2.5.4.

A ¾ inch female Swagelok fitting is used to hold the injector in place. First the threads are bored out so that the o-ring on the injector seals against the fitting. Two 1/8-inch aluminum plates, in conjunction with three 2.5 inch ¼-20 stainless steel bolts, nuts and lock washers, are used to clamp and hold the injector securely in the fitting. A picture of this assembly is provided in Figure 2.5.5.

26
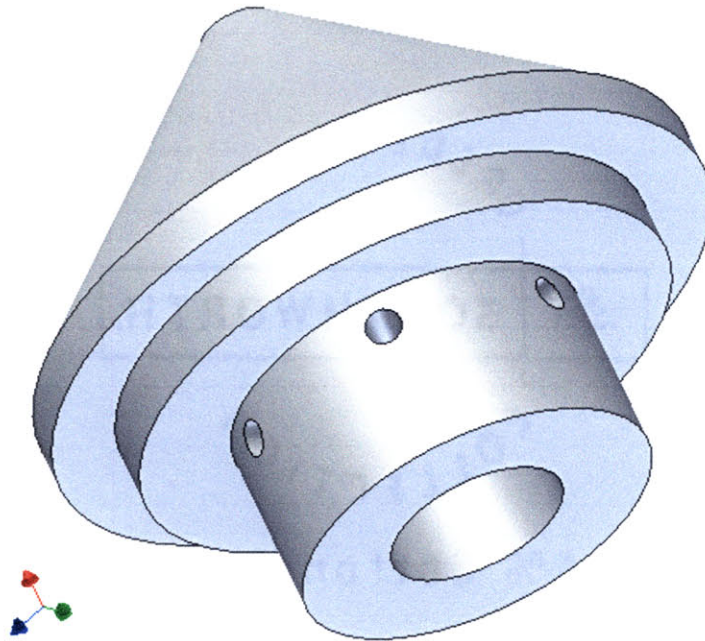
Figure 2.5.3: Redesigned fuel injector nozzle tip.

**Injector Body
and Solenoid**   **Spring**   **Seat Screw**

**Electrical
Connector**   **Brass
                          Washer**   **Plunger**
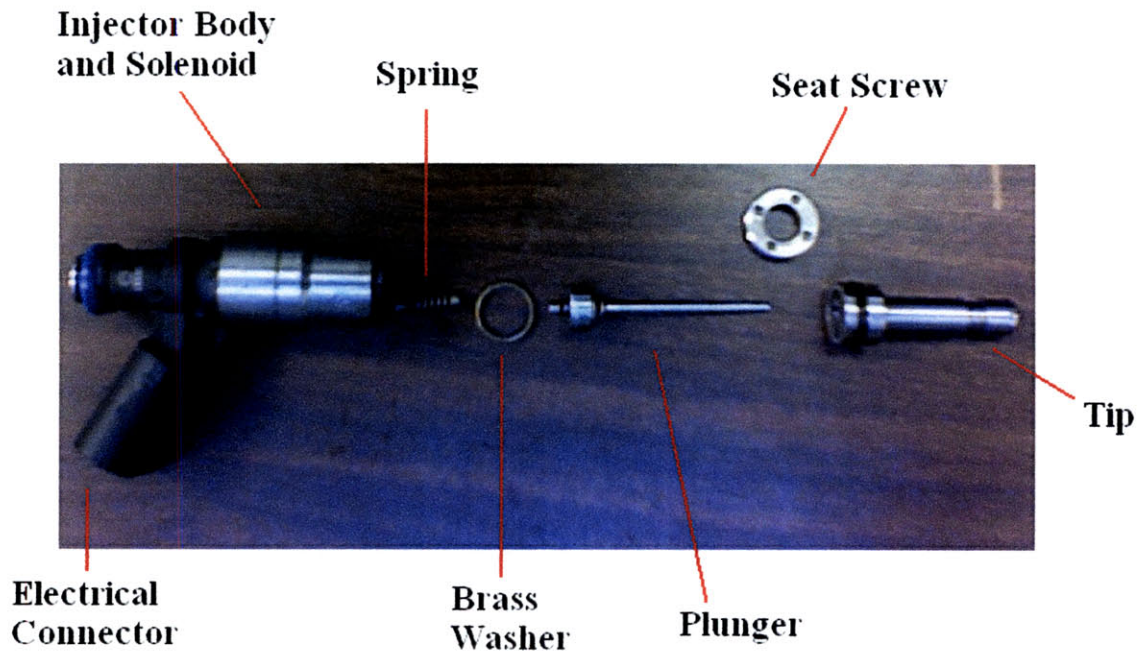
Figure 2.5.4: Exploded view of the fuel injector parts.

Figure 2.5.5: Fuel injector assembly as it sits on the toroidal, fluid supply manifold.

A car battery powers the injectors, while the pulsing is controlled in one of two ways. Initially, along with the injectors, a custom-made Gantec driver was ordered specifically to control the microjet pulsing. Since considerable time passed between receiving the injectors and the driver, earlier tests (for Mach 1.5) were performed with a high-speed relay. For these tests, a National Instruments USB-6008 Multifunction I/O card was used to send a trigger signal. A low voltage signal in the shape of the desired microjet output was sent to a Crydom D06D80 solid-state relay. Opening and closing this relay opens and closes a circuit. This circuit connects a Delco valve-regulated, lead-acid, 12 V battery to the injectors, which are wired in parallel. The injectors open and close with the same frequency and duty cycle as the trigger signal. When the Gantec driver arrived, it was used to pulse the microjets. This driver ensures that enough current is supplied to the injectors to open them properly. It does this by providing a direct current source equivalent to one produced in an automobile by the ignition coil and

distributor. The driver controls the frequency of pulsing as well as the duty cycle. It supports simultaneous firing, as well as batch phase and staggered firing. For the purpose of this investigation, only simultaneous firing was used.

2.6 Anechoic Chamber

The nozzle itself is located in a fully anechoic chamber and the jet exhausts there. The chamber measures 5.2 m wide, 5.8 m long and 4.0 m high. On the opposing wall to the nozzle is an acoustically treated exhaust duct that routs the flow up to the roof of the facility. The walls, ceiling, floor and door are all fully covered with sound-absorbing wedges. Each wedge panel houses three wedges that measure 304.5 mm high, 609.6 mm long and 203.2 m wide. The side of the chamber behind the microphone array has grating installed so that key features of the chamber are easily accessible. However, the grating closest to the jet is covered with wedge panels to inhibit acoustic reflection. The room is ventilated so that the jet properly entrains ambient air. Therefore, the temperature in the room never rises above 320 K for the jet conditions described in this thesis. The ambient pressure, temperature and relative humidity are monitored in the chamber in strategic locations.

2.7 Control Room

In the control room three Windows-based PCs control the operation of the jet. One PC controls the airflow, and another controls the burner. The third acquires the acoustic measurements. All three computers run LabVIEW graphical user interface (GUI) programs. For baseline and pulsed measurements, the data acquisition (DAQ) computer collects three seconds of data. For transient tests, it collects seven seconds with the microjets turning on and off three times at a frequency of 0.5 Hz and 50% duty cycle. It also records the start, stop, and microjet on/off times for analysis purposes. At the start of data collection, a signal is sent to the burner computer so that each run can be matched with its corresponding ambient conditions.

2.8 Acoustic Measurement

Twelve Brüel & Kjær (B&K) model 4939 ¼-inch condenser microphones were used to acquire all of the acoustic data. Figure 2.8.1 is a schematic of a simple condenser microphone. The microphone basically consists of two parallel plates, like a capacitor, though one plate is mounted while the other is free to move on a membrane. A voltage is supplied to the movable plate and the voltage on the stationary plate is measured. This change in voltage corresponds to a specific pressure, based on the microphone's sensitivity. The microphones sit in a 3.048 m circular array in the same plane as the jet, with the center at the nozzle exit. Each microphone is referred to by its radial angle with respect to the nozzle exit and upstream direction. Figure 2.8.2 shows the microphone locations inside the chamber.
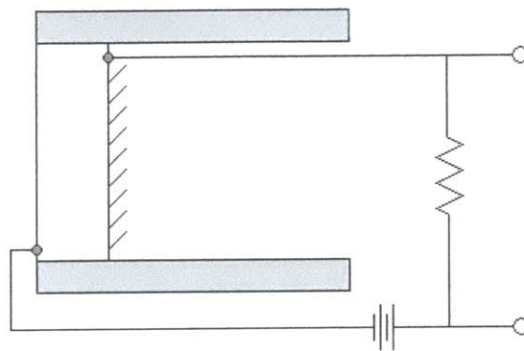
Figure 2.8.1: Simple schematic of a condenser microphone.

Each microphone connects directly to a B&K model 2670 preamplifier. This amplifier has a 2 m cord that terminates at a 7-pin male LEMO connector. Four microphone/preamplifier pairs connect directly into a B&K Nexus 2960 conditioning amplifier; three conditioning amplifiers are used in all to handle all twelve microphones. The microphone sensitivity and polarity is programmed, through the menus on the front screen, directly into the conditioning amplifiers. The acoustic measurements are also low-pass filtered by the conditioning amplifiers with a cutoff frequency of 100 kHz, which is the upper limit of the microphone bandwidth.
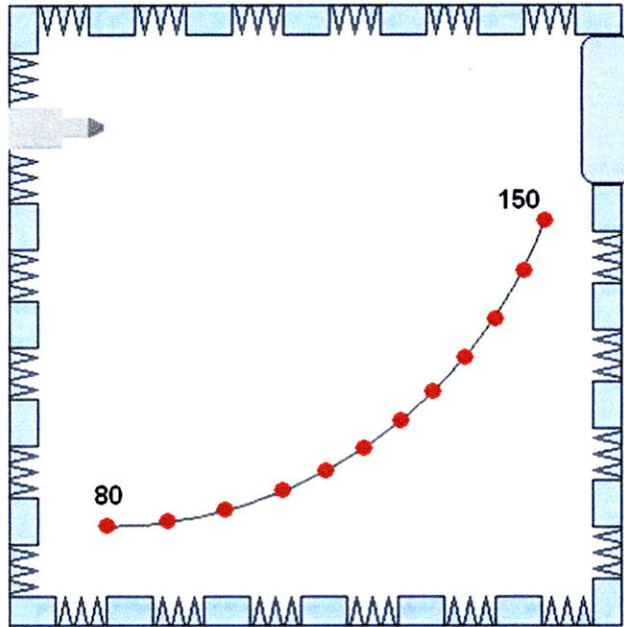
Figure 2.8.2: Microphone locations within the anechoic chamber.

Each amplifier channel outputs to a female BNC connector. Coaxial cables then transfer the signal from the conditioning amplifiers in the anechoic chamber to the data acquisition cards in the control room. These cables are terminated with male BNC connectors. Three National Instruments PCI-6110 high-speed data acquisition cards then connect to the DAQ computer. Each card has four analog input channels so in all 12 channels may be sampled simultaneously. The cards have a maximum sampling frequency of 5 MHz, though each microphone is sampled at 204,800 Hz. The voltage output of each microphone is plotted on the front panel of the DAQ GUI program so that a quick visual inspection may be performed before saving. The data is corrected using the microphone calibration values and converted to pressure (in Pascals) before saving.

2.9 Calibration

Calibration of the microphones is performed using a B&K model 4220 Pistonphone. The pistonphone produces a very accurate 250 Hz signal at 124 dB. The pistonphone has a ¼-inch opening at one end, which is placed over each microphone one at a time. Its weight is supported by a stand that was fabricated in-house. A signal was collected from each microphone by a LabVIEW based program and the computed SPL value was compared to the 124 dB known SPL. A correction value was found and stored

in a correction file. During data acquisition, the program calls this file and automatically adjusts each microphone signal accordingly.

Though very accurate, calibrating with the pistonphone can prove to be extremely time consuming. Therefore, to verify the initial calibration, and thus cut the calibration time, a technique called Charge Injection Calibration (CIC) was used. Within the conditioning amplifier, a small capacitance is introduced—typically 0.2 pF, with a very high leak impedance (50 TΩ). Then a known reference signal is introduced at one of several given frequencies. The resulting measured response is compared with the stimulus and a CIC gain is found from the RMS values. Given the properties of the CIC capacitance, even small changes in the measurement chain cause extreme changes in the CIC gain. As a result, given the fact that no major changes to the CIC gain have occurred, the original calibration values can be verified, and a new calibration need not be performed. Another advantage of using CIC is that changes in the entire measurement chain (not just within the microphone and preamplifier) are detected. Therefore by testing several frequencies, the exact cause of the change (be it a problem with the microphone or a faulty cable) may be diagnosed.

CHAPTER 3

EXPERIMENTAL PROCEDURE

3.1 Overview

Three types of tests were performed over the course of this investigation: baseline, steady and pulsed. The following chapter discusses the purpose and procedure for each test, as well as the data processing and analysis techniques used.

3.2 Experimental Description

This section describes the basis for each type of experiment. Three types of experiments were conducted to determine the capability of pulsed microjet injection to reduce supersonic jet noise. The three types of tests are described in this section.

3.2.1 Baseline Jet Noise and Steady Microjet Injection

The term "baseline" refers to a test performed with no external noise suppression techniques. It is the pure noise profile one would expect when measuring the noise produced from a real jet engine. The efficacy of each noise reduction technique was measured based on the total baseline noise produced by the jet at its operating condition. Therefore, baseline tests play a critical role in this investigation.

Previous work with microjets was performed using a steady injection condition. Using this method, a noise reduction of up to eight dB could be achieved. This quantity refers to the reduced noise as compared with the baseline noise in the peak radiation direction. The effectiveness of any noise reduction technique is measured against the steady injection noise reduction.

3.2.2 Pulsed Microjet Testing

As a starting point for pulsed microjet testing, initial results are desirable. There are several parameters that require attention—the most prominent being that microjets require a fluid with weight and volume that would presumably need to be carried on board the aircraft. Different types of fluids may be used, such as air and water, but heavier fluids prove to be more effective at reducing noise. As such, maximizing noise reduction while minimizing fluid usage would be a central goal. This is especially true when the working fluid is water. Though it is 1000 times denser than air, its use as the injected fluid produces the largest reduction in noise. Initial testing on this idea would be highly desirable. By comparing pulsed microjet injection to steady injection, and measuring the corresponding injection flow rates, one would be able to determine whether comparable results could be achieved with less fluid flow.

3.3 Experimental Procedure

As stated in section 2.1.7, three computers located in the control room operate the facility. One computer runs a program for monitoring the SUE burner and another runs a separate program that controls the airflow through the facility. The third computer is the DAQ computer. It runs a third, separate program that simultaneously operates the microjets and obtains acoustic measurements. Operation of the hot jet facility requires at least two people. The first monitors the burner and flow control computers, as the user interfaces are located at one workstation. The second is responsible for the DAQ and microjet control computer.

Each operation condition consists of a given pressure ratio and temperature. Once the burner is lit and sufficiently warmed up, temperature control is turned on. This consists of a controller that adjusts the main fuel valve, based on the temperature read by thermocouples downstream of the burner, allowing more fuel for higher temperatures. As such, the pressure ratio may be adjusted easily and the temperature will self-adjust to the target value. The first operator adjusts the air supply settings until the jet is running steadily at the operating condition, then signals to the second operator that condition is reached. At that point, the second operator starts the data acquisition program. At the

start of the program, a signal is sent to the flow control program, which logs the instantaneous room humidity, ambient pressure and temperature. The program then takes three seconds of data simultaneously on all twelve microphones. The program then prompts the second operator to save the data to an appropriately named file. Control parameters and file names are entered prior to program initiation. Once the data has been saved, the second operator signals to the first that it is okay to move to the next operating condition.

3.4 Data Processing and Analysis

In collecting acoustic data, the overall sound pressure level is the most obvious indicator of the noise generated by a jet, as well as the amount of noise reduction achieved. This value is derived from the frequency spectra obtained from the raw pressure data. The methods by which the frequency spectra and overall sound pressure level were calculated are described in the following section. Also discussed is the technique by which the flow rates through the injectors were measured.

3.4.1 Frequency Spectrum

In order to compare noise reductions, it is necessary to convert the pressure-time signal (the form in which it arrives from the microphones) into a single overall sound pressure level (OASPL) value. This is a catchall value that, in effect, is a measure of the magnitude of the noise at a given location. Derived from the frequency spectrum, its computation uses the methodology described in Bendat and Piersol [14]. First discussed will be the computation of the frequency spectrum.

The microphones are sampled at for three seconds at a frequency of 204,800 Hz. At each microphone location, this gives a total of 614,400 samples. First, it is necessary to subtract the mean from the pressure-time signal. This gives a new signal, $p' = p - \bar{p}$, which has a zero mean, from which it is easier to calculate the frequency spectrum. It is computationally advantageous, at this point, to divide p' into subsets of equal size. Choosing a subset size of a power of two ensures that the subsequent Fourier transforms are simple to perform. Therefore, in this case, the subset size is chosen as 4096, or 2^{12}. Then, to increase the number of subsets, the data is overlapped by 50%. This gives a

total of $2\left(\dfrac{N}{n_s}\right) - 1 = 2\left(\dfrac{614,400}{4096}\right) - 1 = 299$ subsets. Before a Fourier transform is performed, the subsets are windowed using a Hanning window, which is defined by $w_h = 1 - \cos^2\dfrac{\pi t}{T}$, where T is the length of the subset, or 4096, and t is the index of the sample. The subsets are windowed in order to reduce side lobe leakage, and are thus ready for Fourier transformation. Using the Cooley-Tukey procedure, each windowed subset is transformed. The subset is then multiplied by the Hanning scale factor of $\sqrt{\dfrac{8}{3}}$.

Each value in the transformed subset is then multiplied by its complex conjugate to ensure that the entire subset contains only real parts. Then all the subsets are averaged, and a spectrum is obtained. The spectrum has units of [pressure^2/frequency]. Using the notation in Bendat and Piersol [14], the one-sided autospectral density function is then estimated by

$$\hat{G}_{pp}(f_k) = \begin{cases} \dfrac{2}{n_d N \Delta t} \sum_{i=1}^{n_d} |P_i(f_k)|^2 & k = 1,2,3,\dots,[(N/2-1)] \\[4mm] \dfrac{1}{n_d N \Delta t} \sum_{i=1}^{n_d} |P_i(f_k)|^2 & k = 0,(N/2) \end{cases} .$$

Multiplying $\hat{G}_{pp}$ by the frequency spacing, $\Delta f = \dfrac{f_s}{n_s} = \dfrac{204,800}{4096} = 50$, gives the autospectral density function with units of [pressure^2]. The final step is then to calculate the frequency spectrum in terms of the sound pressure level (SPL) by

$$SPL(f_k) = 10 \cdot \log\left(\dfrac{\hat{G}_{pp}(f_k)}{p_{ref}^2}\right),$$ where p_{ref} is defined as 20 μPa.

3.4.2 Overall Sound Pressure Level

The overall sound pressure level is calculated from the autospectral density function discussed in the last section. The autospectral density function is integrated numerically by Simpson's method using the frequency spacing, Δf, as the step size.

This value, referred to as p_{rms}^2, has units of [pressure^2]. The final OASPL value is then calculated by $OASPL = 10 \bullet \log\left(\dfrac{p_{rms}^2}{p_{ref}^2}\right)$, where p_{ref} is again defined as 20 µPa.

3.4.3 Injector Flow Rates

A rather elementary, but effective, method was used to determine the flow rate of water through each injector for various pulsing frequencies, duty cycles and injection pressures. Programmed to operate the injector for three seconds exactly, a computer was used to pulse the injector (or keep it open) at the requested frequency and duty cycle. Pressure was applied to the inlet of a water tank and measured by means of a high-pressure gas supply and regulator valve. The wired injector was installed on the exit of the water tank. The water ejected during the operation period was collected in a beaker of known mass, and the mass of the water was determined using a triple-beam balance. Dividing this mass by three seconds yields the mass flow rate.

3.5 Error Estimates

Great care was taken in the design of the facility and of the data acquisition systems used in the collection of this data. Therefore, few sources of error and uncertainty exist. However, this section discusses the few remaining uncertainties and their effect on the results.

3.5.1 Acoustic Uncertainty

While there are several schools of thought regarding uncertainty, the absolute uncertainty, which gives the worst-case scenario, is presented. Since the microphone response is taken into account in the data acquisition program, and is factored even before saving, the only remaining uncertainties lie with the resolution of the DAQ cards in conjunction with the gains specified by the card and the amplifier. The worst-case scenario with respect to uncertainty occurs when the input range is set to ±10 V and the amplifier gain is set to 3.16 mV/Pa (its lowest value). Since the DAQ resolution is constant (12 bit), the uncertainty in pressure is obtained by the following:

$$\varepsilon_p = \frac{1}{2}\frac{range}{resolution}\frac{1}{gain} = \frac{1}{2}\left(\frac{20V}{4096}\right)\frac{1}{3.14\,mV\!\!\Big/_{Pa}} = 0.77\,Pa.$$

For the range that is most important to this study, that around 130dB, this corresponds to an uncertainty of ±0.1 dB.

3.5.2 Flow Measurement Uncertainty

The program in control of the flow rate experiments is designed to operate the valve for only three seconds. At the frequencies of interest, this allows for only 3, 15 or 30 pulses. So there is no uncertainty with respect to the length of time the injectors fire. However, the injectors do not seal completely (since they were modified from their original geometry) and leak very slightly. The amount of fluid leaked depends on the supplied pressure. However, since the density of water is 1 mg/cm^3, and the number of drops surrendered by the injector is much less than 100, the water injected is two to three orders of magnitude larger than the lost water (depending on the measured mass of the collected water). Therefore the dripping may be neglected.

CHAPTER 4

RESULTS

4.1 Baseline Noise

Since this work concentrates on jet noise reduction, it is important to start first by presenting a solid set of baseline data. This step is crucial, since all of the reported results are compared directly with the baseline data. Figure 4.1.1 shows baseline OASPL values for an ideally expanded Mach 1.8 jet. Each run condition (900°F, 1300°F and 1700°F) is presented.

In addition, Figure 4.1.2 presents an alternate set of baseline data alongside that presented in Figure 4.1.1. This not only shows consistency and repeatability between experiments, but congruency between this data and that obtained previously (Greska). These baseline data are obtained at the start of each run. During the same run, several sets of data are recorded after the baseline. Therefore, each set of data acquired using microjets is compared to the baseline set from its same run. This ensures that the noise reduction associated with microjet injection is matched best with the run condition.
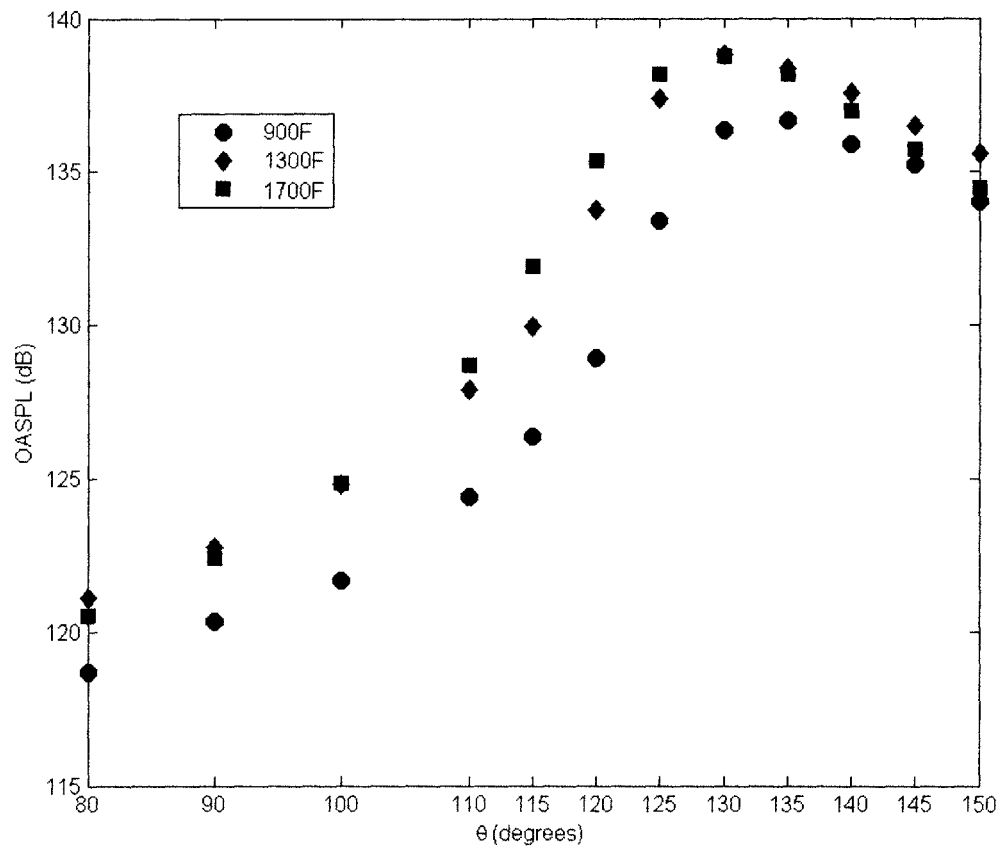
Figure 4.1.1: Baseline OASPL values as a function of angle at each of the operating temperatures of a Mach 1.8 jet.
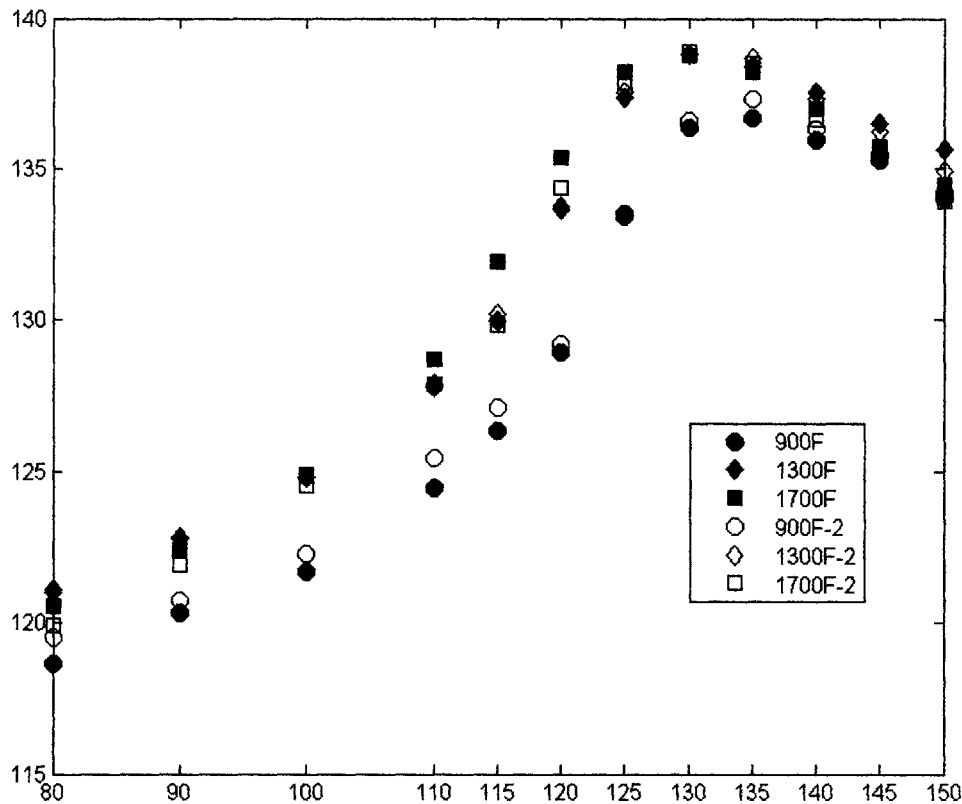
Figure 4.1.2: Alternate set of baseline OASPL values as a function of angle at each of the operating temperatures of a Mach 1.8 jet. The alternate set is tagged with a "-2" and presented with open symbols.

4.2 Noise Reduction Using Pulsed Microjet Injection

In this section results related to the noise reduction of a Mach 1.8 jet at 900, 1300 and 1700°F due to pulsed microjet injection are presented. The microjets were pulsed at 1, 5 and 10 Hz, with injection pressures of 400 and 800 psi[1], and a duty cycle[2] of 50%. Duty cycle and its effects are discussed further in section 4.4.

Figure 4.2.1 shows the noise reduction at 900°F as a function of angle for steady and pulsed microjet injection. First, we note that in the peak radiation direction, steady injection at 800 psi achieves a reduction of over 2 dB, whereas over 1 dB of noise reduction is seen with 400 psi injection. Comparatively, with pulsing at 800 psi, about

---

[1] From here on, all references to pressure will correspond to gauge pressure.
[2] The term "duty cycle" refers to the amount of time the valve spends open relative to the frequency at which it is operating. It is given in terms of a percent, which is the fraction of overall time the valve remains open.

41

60% of the noise reduction as compared to steady injection at the same pressure is achieved. This corresponds to a reduction of over 1 dB. With pulsing at 400 psi, about 47% of the noise reduction as compared to steady injection at the same pressure is achieved. This corresponds to a reduction of 0.5 dB. Since the level of noise reduction is a function of not only the injection pressure but the injection mass flow rate, it is necessary to compare the amount of water used by pulsed and steady microjets. At 800 psi, pulsing achieves 60% of the noise reduction as compared to steady injection at the same pressure, but uses only 38% of the water. At 400 psi, pulsing achieves 47% of the noise reduction as compared to steady injection at the same pressure, but consumes only 47% of the water.
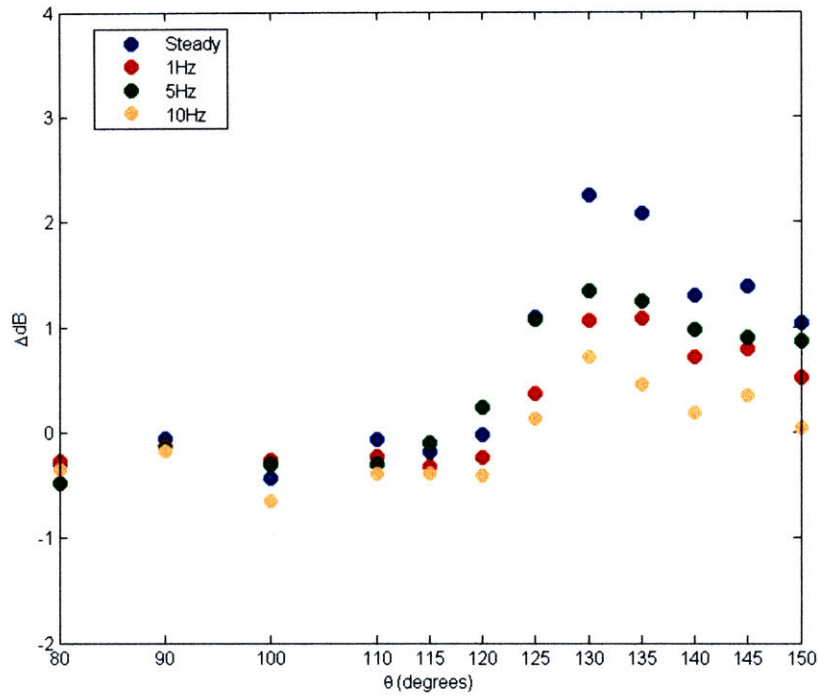
Figure 4.2.2 shows the noise reduction at 1300°F as a function of angle for steady and pulsed microjet injection. First, we note that in the peak radiation direction, steady injection at 800 psi achieves a reduction of over 3 dB, whereas over 2 dB of noise reduction is seen with 400 psi injection. By comparison, with pulsing at 800 psi, about 78% of the noise reduction as compared to steady injection at the same pressure is achieved. This corresponds to a reduction of about 2 dB. With pulsing at 400 psi, about 70% of the noise reduction as compared to steady injection at the same pressure is achieved. This corresponds to a reduction of about 1.5 dB. Comparing water usage, we see that pulsing at 800 psi achieves 78% of the noise reduction as compared to steady injection at the same pressure, but uses only 38% of the water. At 400 psi, pulsing achieves 70% of the noise reduction as compared to steady injection at the same pressure, but consumes only 47% of the water.

Figure 4.2.3 shows the noise reduction at 1700°F as a function of angle for steady and pulsed microjet injection. First, it should be noted that in the peak radiation direction, steady injection at 800 psi achieves a reduction of over 3 dB, whereas about 1 dB is achieved with 400 psi injection. Comparatively, pulsing at 800 psi produces 37% of the noise reduction as compared to steady injection at the same pressure. This corresponds to a reduction of about 1 dB. With pulsing at 400 psi, about 90% of the noise reduction as compared to steady injection at the same pressure is achieved. This corresponds to a reduction of about 1 dB. Again, it is necessary to take note of the flow rates corresponding to these reductions. Pulsing at 800 psi achieves 37% of the noise

reduction as compared to steady injection at the same pressure, but uses only 38% of the water. At 400 psi, pulsing sees 90% of the noise reduction associated with steady injection at the same pressure, but consumes only 47% of the water.

One might be tempted to conclude from the above discussion that pulsing only achieves a fraction of the noise reduction of steady microjet injection. It should be noted, however, that pulsing achieves these reductions while using an even smaller fraction of the water that steady microjets consume.

Also, it should be noted that at 900°F, pulsing at 5 Hz produced the best results for injection at 800 psi, and at 400 psi 10 Hz pulsing was most effective. However, at 1300°F, the optimum frequency was 1 Hz for injection at both 800 and 400 psi. At 1700°F, the optimum frequencies were observed to be 1 and 5 Hz for injection at 800 and 400 psi respectively.

(a)
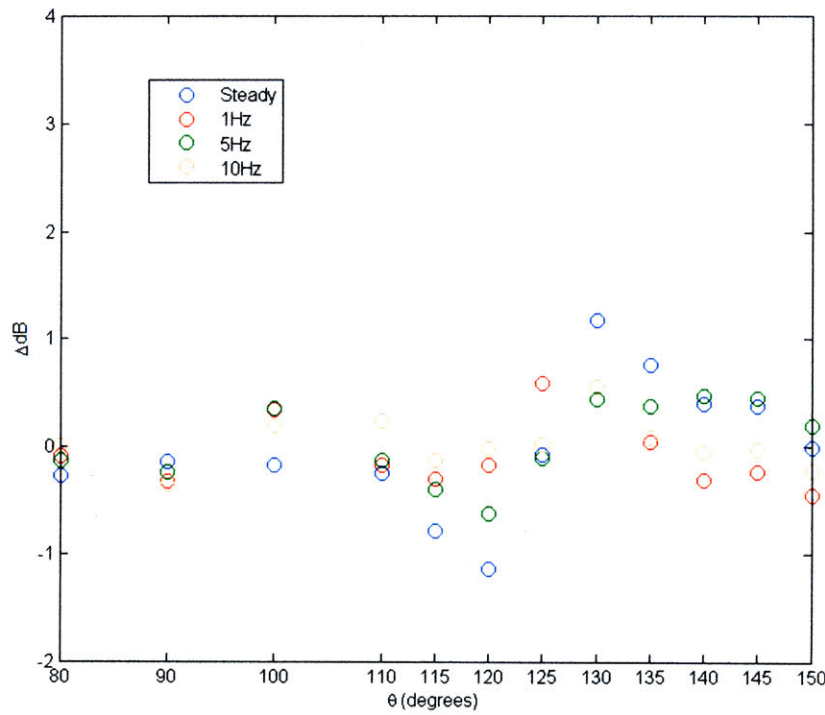
(b)

Figure 4.2.1: Total noise reduction of a Mach 1.8 jet at 900°F using aqueous microjet injection at (a) 800 psi and (b) 400 psi with a duty cycle of 50%.
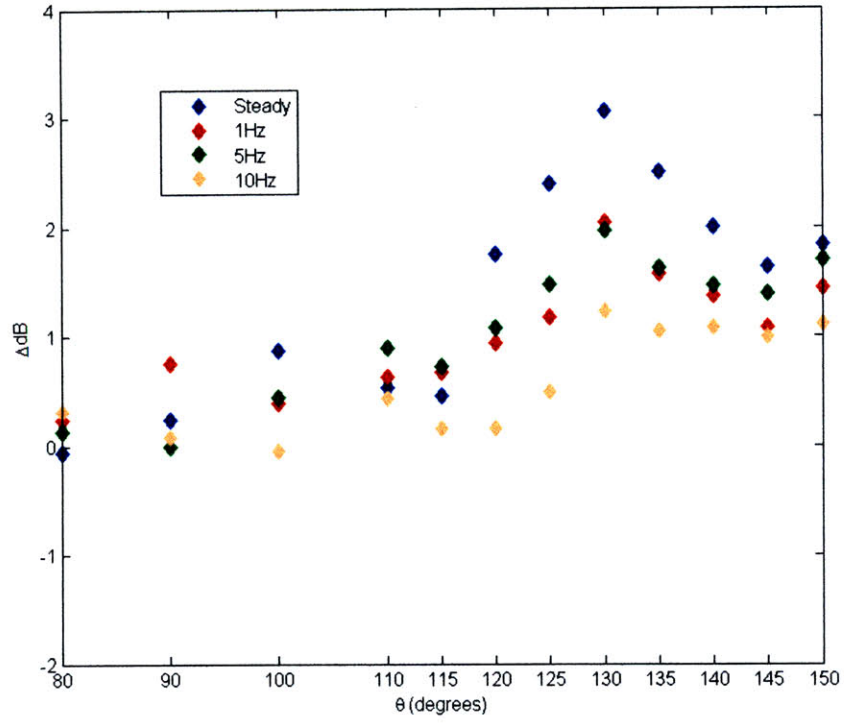
(a)
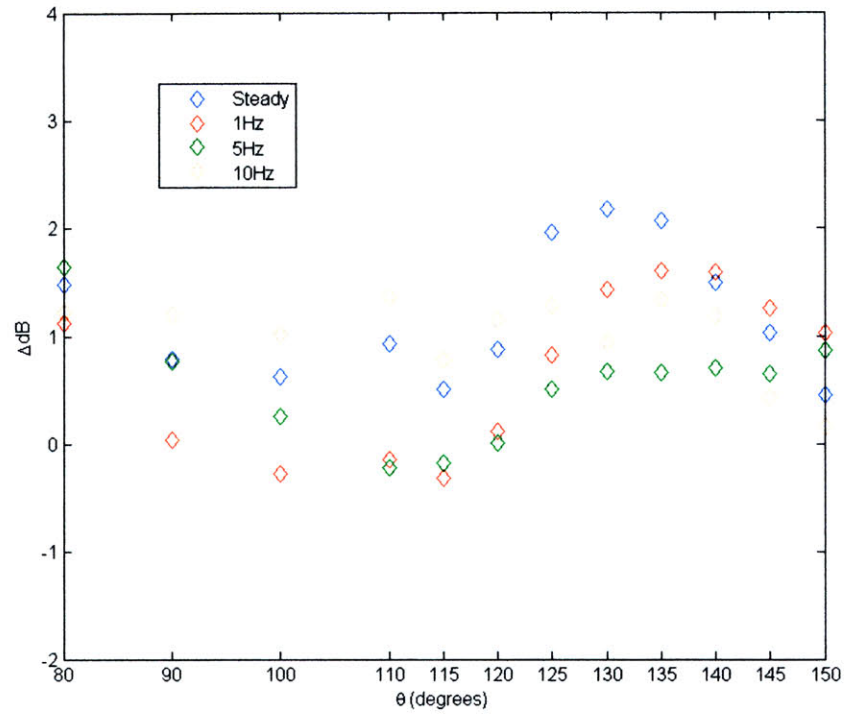
(b)

Figure 4.2.2: Total noise reduction of a Mach 1.8 jet at 1300˚F using aqueous microjet injection at (a) 800 psi and (b) 400 psi with a duty cycle of 50%.

45
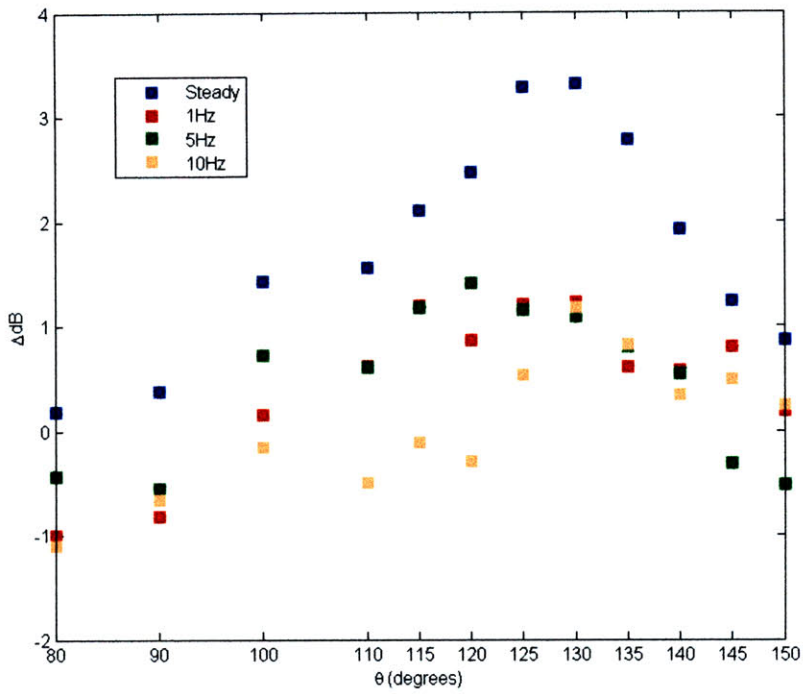
(a)
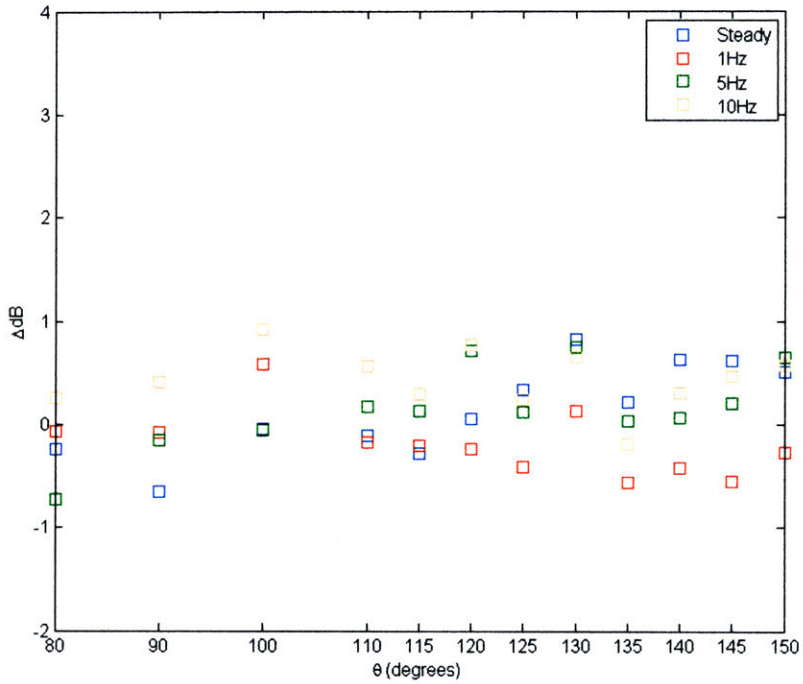
(b)

Figure 4.2.3: Total noise reduction of a Mach 1.8 jet at 1700˚F using aqueous microjet injection at (a) 800 psi and (b) 400 psi with a duty cycle of 50%.

4.3 Supersonic Jet Noise Reduction and Water Usage

At this point it is prudent to compare things in a different manner. With the primary goal being to achieve the same noise reduction using less water, comparing noise reductions in the peak radiation direction with the amount of water used would make the most sense. Therefore, the mass flow rate is considered as the variable of primary interest.

Figure 4.3.1: Noise reduction in the peak radiation direction of a Mach 1.8 jet at 900°F as a function of mass flow rate through each injector.

The noise reduction of a Mach 1.8 jet at 900°F in the peak radiation direction is presented in Figure 4.3.1 as a function of the mass flow rate through each injector. At first, the presented data seems to follow a weak, positive, linear trend. However, there are two key pieces of information here: first, pulsing at 5 Hz at a pressure of 800 psi (corresponding to point A) yields more noise reduction than steady injection at 400 psi

(corresponding to point B), and second, the former condition requires only about 66% as much water as the latter.

Figure 4.3.2 shows the noise reduction in the peak radiation direction for a Mach 1.8 jet at 1300°F as a function of mass flow rate through each injector. From this figure it is seen that pulsed injection at 800 psi and a frequency of 1 Hz (corresponding to point A) reduces noise by an amount comparable to that when steady microjets at 400 psi are used (corresponding to point B). And again, only about 66% of the water is used when pulsing.
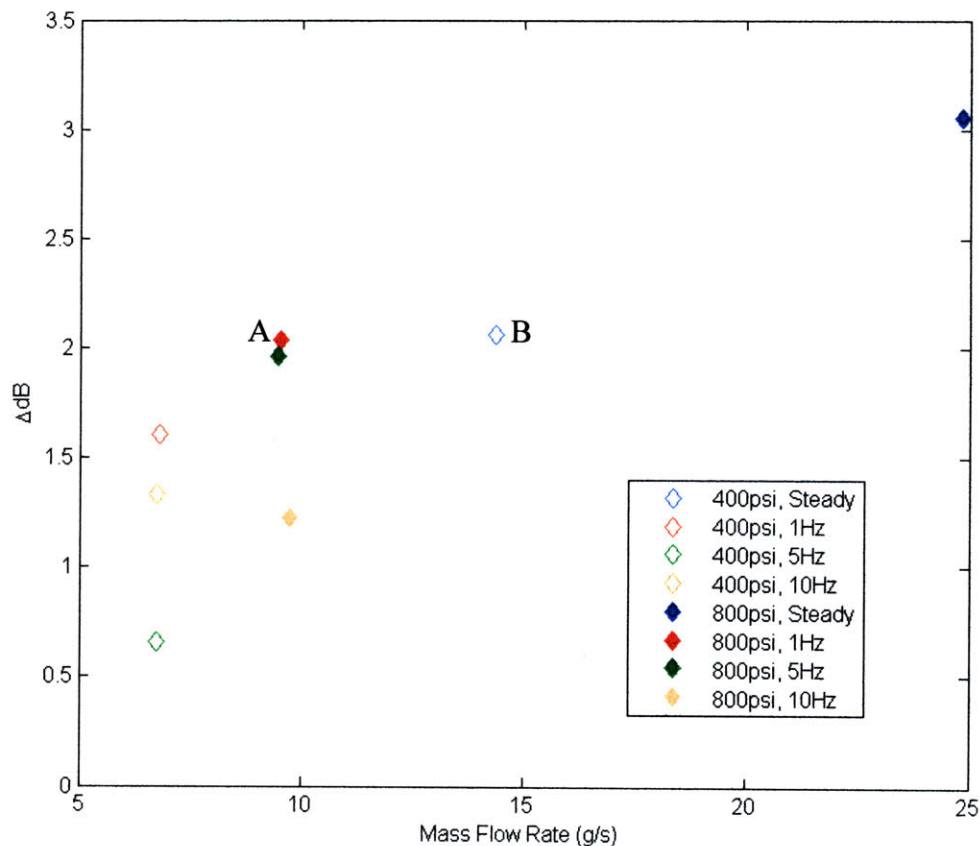
Figure 4.3.2: Noise reduction in the peak radiation direction of a Mach 1.8 jet at 1300°F as a function of mass flow rate through each injector.

The noise reduction achieved by a Mach 1.8 jet at 1700°F is presented in Figure 4.3.3 as a function of mass flow rate. Interestingly, all three pulsing frequencies at 800 psi (corresponding to the grouping of points labeled A) produce a noise reduction

significantly greater than that when using 400 psi steady microjets (corresponding to point B). Again, only 66% of the water is used when pulsing.
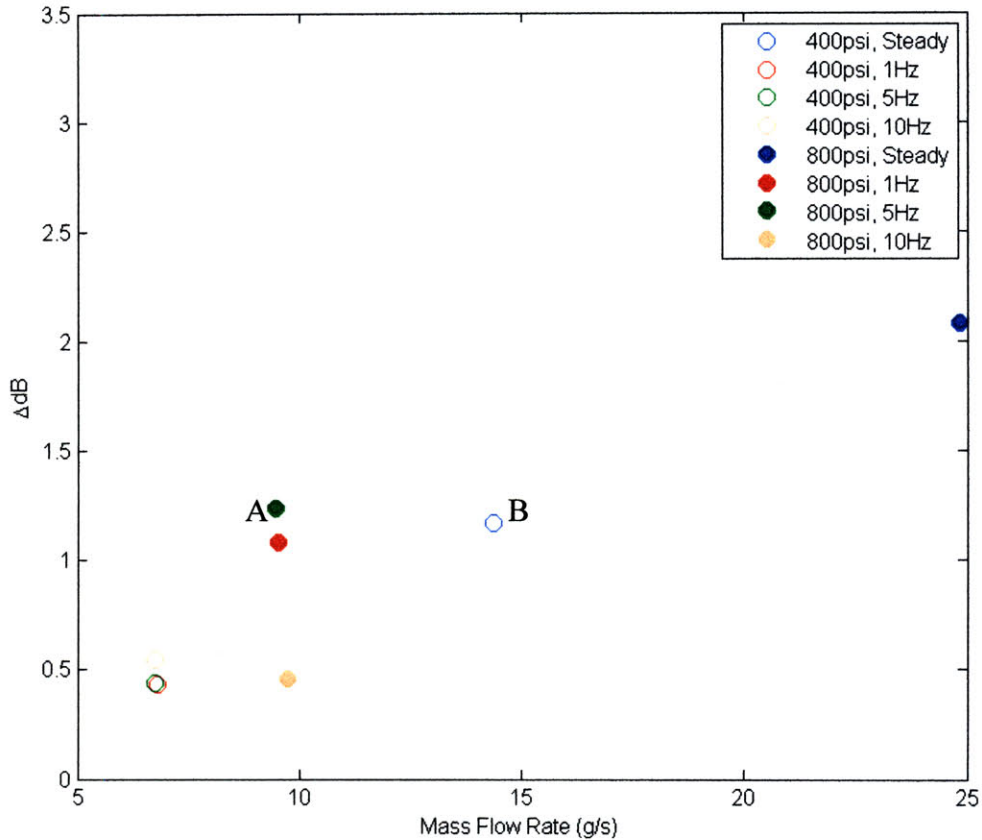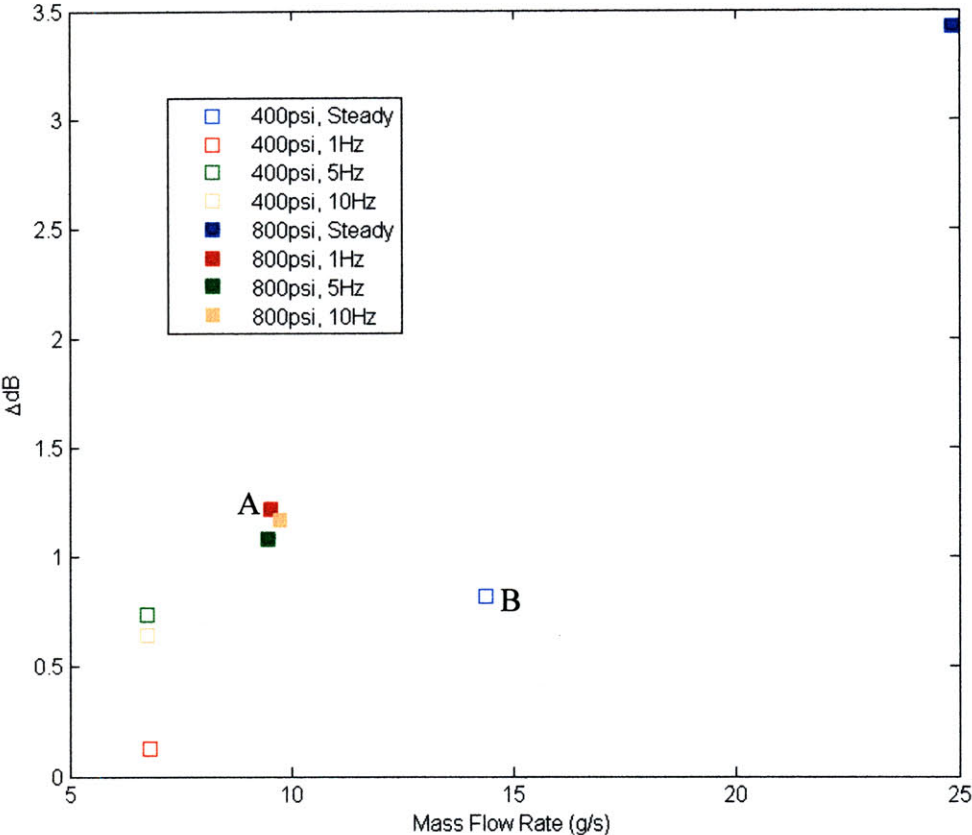

Figure 4.3.3: Noise reduction in the peak radiation direction of a Mach 1.8 jet at 1700˚F as a function of mass flow rate through each injector.

4.4 Duty Cycle and Its Effect on Noise Reduction

Up to this point, all pulsing has been conducted with a 50% duty cycle. This simply means that for every open-close cycle, the valve stays open for half the time, then remains closed the other half. In order to investigate the effects of duty cycle on noise reduction, the aforementioned experiments were repeated with the same conditions, save for the pulsing duty cycle, which was changed to 75%. This means that the valve remains open 75% of the time and stays closed for 25% relative to the frequency at which it is operating.

Figure 4.4.1 shows the noise reduction achieved as a function of direction for a Mach 1.8 jet operating at 900˚F. Though the noise reduction achieved through pulsed

microjet injection still falls short of steady injection, it is much more significant in this case. In the peak direction of 135°, pulsing at 10 Hz with a duty cycle of 75% produces almost as much noise reduction as with steady injection.
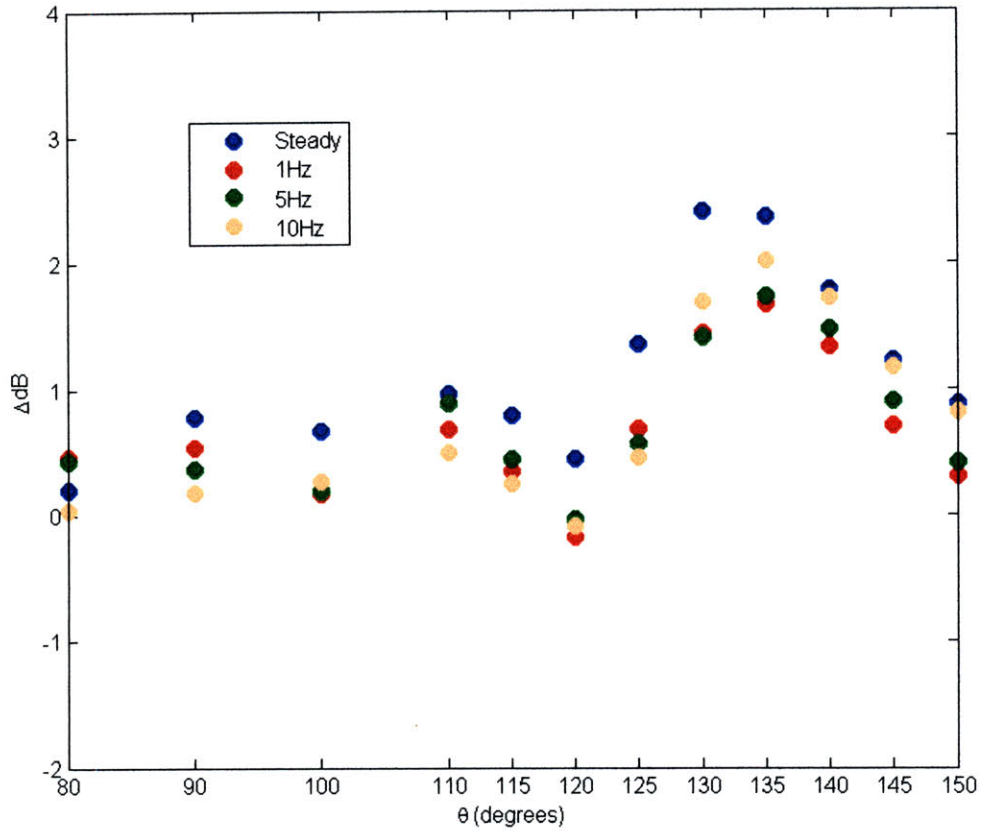
Figure 4.4.1: Total noise reduction of a Mach 1.8 jet at 900°F using aqueous microjet injection at 800 psi with a duty cycle of 75%.

The noise reduction of a Mach 1.8 jet at 1300°F is plotted in Figure 4.4.2 as a function of direction. Once again, in this case, the greatest noise reduction returns to the peak direction of 130°. It appears, in this case, that in reducing the duty cycle from 100% to 75%, one need only sacrifice 0.5 dB. This of course comes with the advantage that less water is used. In the 900°F case, it seems that 10 Hz produces the greatest pulsed noise reduction. In the 1300°F case, however, 5 Hz seems to be the most advantageous frequency when choosing pulsing.
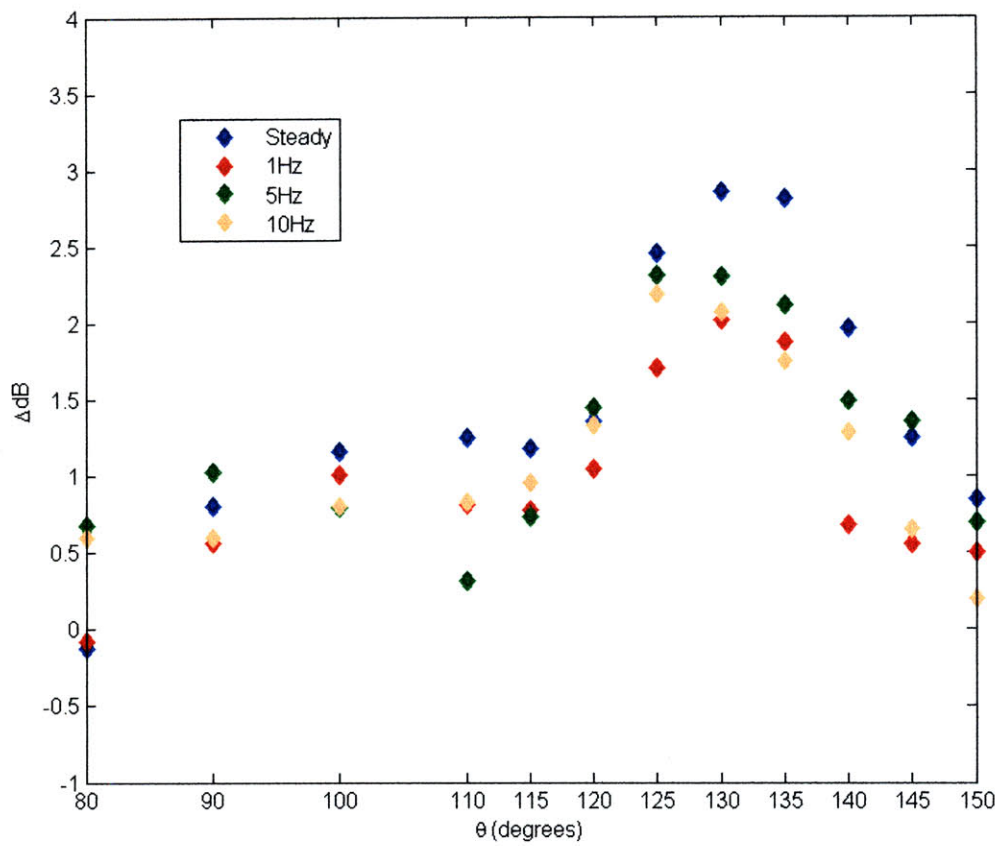
Figure 4.4.2: Total noise reduction of a Mach 1.8 jet at 1300°F using aqueous microjet injection at 800 psi with a duty cycle of 75%.

Finally, Figure 4.4.3 shows the noise reduction of a Mach 1.8 jet operating at 1700°F as a function of direction. The noise reduction in this case suffers slightly as a result of the duty cycle cut from 100% to 75%. However, pulsing at 10 Hz still produces a formidable reduction. It should be noted that for all of these cases, the flow rate associated with pulsing at 75% duty cycle, regardless of the frequency, is still less than the flow rate through steady microjets at 400 psi.
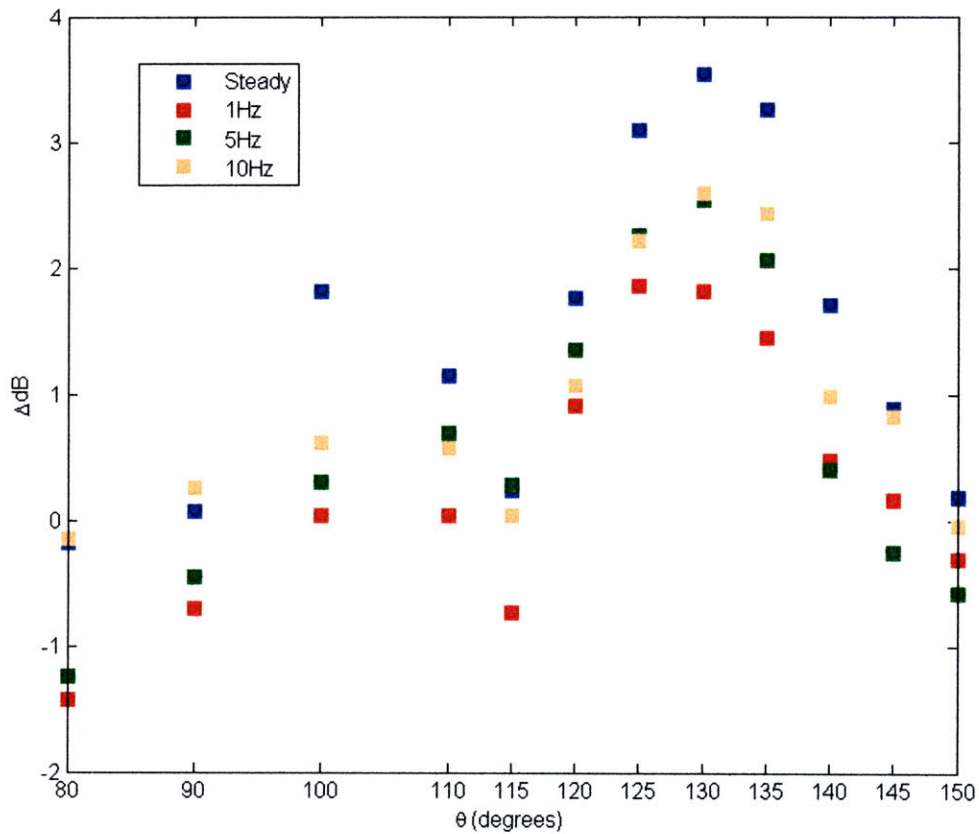
Figure 4.4.3: Total noise reduction of a Mach 1.8 jet at 1700°F using aqueous microjet injection at 800 psi with a duty cycle of 75%.

The noise reductions for a Mach 1.8 jet presented in this section in the peak direction are plotted in Figure 4.4.4 as a function of mass flow rate. For the 900 and 1700°F cases, all three pulsing frequencies produce more noise reduction than steady injection at 400 psi, even though less water is used. For the 900°F case, it can be seen by comparing points A and B in Figure 4.4.4 (a), that nearly twice as much noise reduction is obtained while using only 90% of the water. For the 1700°F case, it can be seen from Figure 4.4.4 (c) by comparing points A and B, that nearly three times the noise reduction

is obtained while only using 90% of the water. For the 1300°F case, it can be seen from Figure 4.4.4 (b) that pulsing at 1 Hz produces comparable results while 5 and 10 Hz (5 Hz corresponding to point A) produce more noise reduction than steady injection at 400 psi (corresponding to point B), even though less water is used. The same noise reductions are achieved while only using 90% of the water.
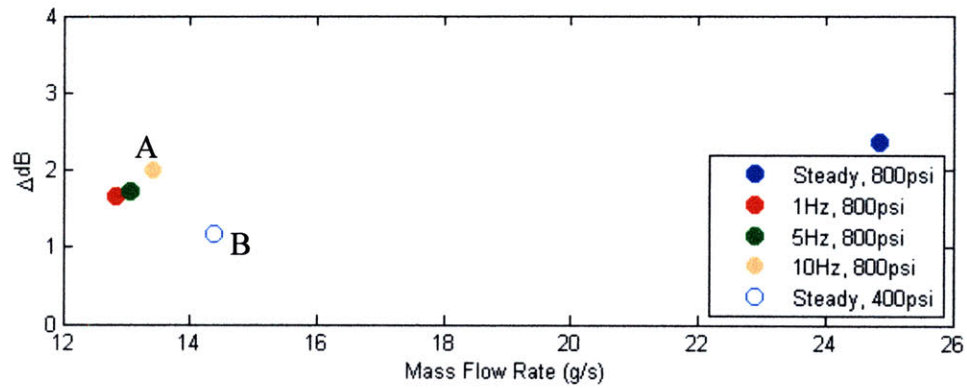
(a)
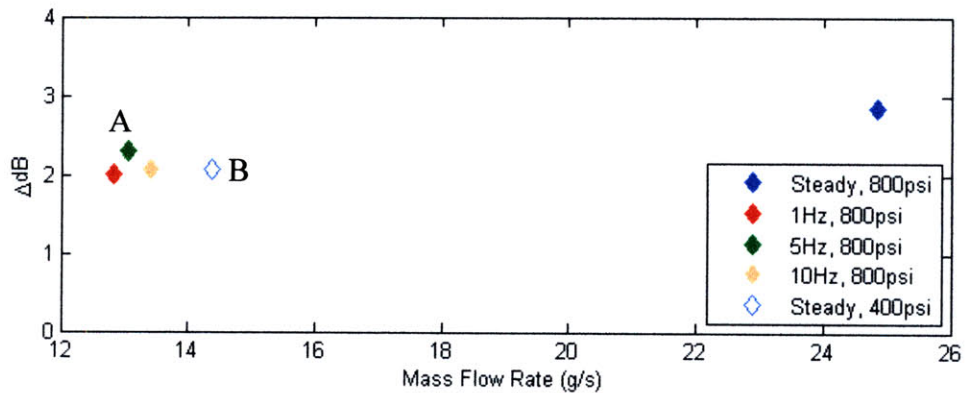
(b)
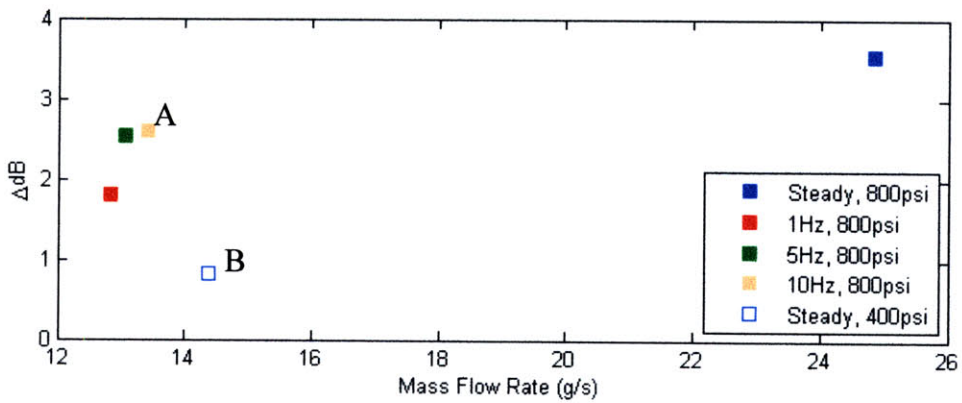
(c)

Figure 4.4.4: Noise reduction using steady injection and pulsing at 75% duty cycle of a Mach 1.8 jet at (a) 900°F, (b) 1300°F and (c) 1700°F as a function of mass flow rate.

Mach 1.8, 400 psi Injection, 50% Duty Cycle						
Frequency	900°F		1300°F		1700°F	
	%ΔdB	%$\dot{m}$	%ΔdB	%$\dot{m}$	%ΔdB	%$\dot{m}$
1Hz	37.3	47.3	77.8	47.3	15.4	47.3
5Hz	37.4	46.9	32.0	46.9	90.2	46.9
10Hz	46.9	46.9	64.4	46.9	78.9	46.9

(a)

Mach 1.8, 800 psi Injection, 50% Duty Cycle						
Frequency	900°F		1300°F		1700°F	
	%ΔdB	%$\dot{m}$	%ΔdB	%$\dot{m}$	%ΔdB	%$\dot{m}$
1Hz	52.1	38.4	66.9	38.4	37.0	38.4
5Hz	59.6	38.1	64.3	38.1	32.7	38.1
10Hz	21.9	38.0	40.2	38.0	35.4	38.0

(b)

Mach 1.8, 800 psi Injection, 75% Duty Cycle						
Frequency	900°F		1300°F		1700°F	
	%ΔdB	%$\dot{m}$	%ΔdB	%$\dot{m}$	%ΔdB	%$\dot{m}$
1Hz	70.6	51.7	70.7	51.7	51.2	51.7
5Hz	73.5	52.6	82.9	52.6	71.8	52.6
10Hz	85.3	54.0	72.6	54.0	73.4	54.0

(c)

Table 4.4.5: OASPL reduction and mass flow rate percentages of steady injection values for pulsing at 1, 5 and 10 Hz at the same injection pressure.

The data presented in sections 4.3 and 4.4 are presented again in Table 4.4.5 to better demonstrate the efficacy of pulsed microjet injection as compared to steady

injection. Each OASPL reduction in the peak direction for pulsed injection is divided by the corresponding reduction using steady injection. The amount of water used in each pulsing case is then divided by the amount of water used for steady injection. Therefore, both values are given in terms of a percentage of the value associated with steady injection.

Figure 4.4.6 shows the noise reduction as a function of duty cycle for each operating condition of the Mach 1.8 jet. As one might expect, increasing the duty cycle increases the noise reduction in the peak radiation direction. The data points corresponding to 100% duty cycle were obtained from the steady microjet injection data. As an abuse of the term, and therefore in a very abstract way, steady injection corresponds to a duty cycle of 100%. That is, the valve remains open 100% of the time and stays closed for 0% of the time relative to the pulsing frequency (the value of which is of course immaterial). Each of the other points was chosen based on which frequency gave the best reduction. For the 900°F jet, there appears to be a slight parabolic trend with downward concavity. As the duty cycle is reduced from 100%, the noise reduction would remain relatively high. This would suggest an optimum duty cycle less than 100%. On the other hand, for the 1300°F jet, there appears to be a slight parabolic trend with the opposite concavity. As one varies the duty cycle down from 100%, the noise reduction would fall off relatively quickly, suggesting that the optimum duty cycle remains at 100%. For the 1700°F jet, a slight parabolic trend with downward concavity appears to exist, again suggesting, as for the 900°F case, that the optimum duty cycle resides somewhere less than 100%.

3.5

● 900F
♦ 1300F
■ 1700F

3

2.5

ΔdB

2

1.5

1

50   75   100
Duty Cycle (%)
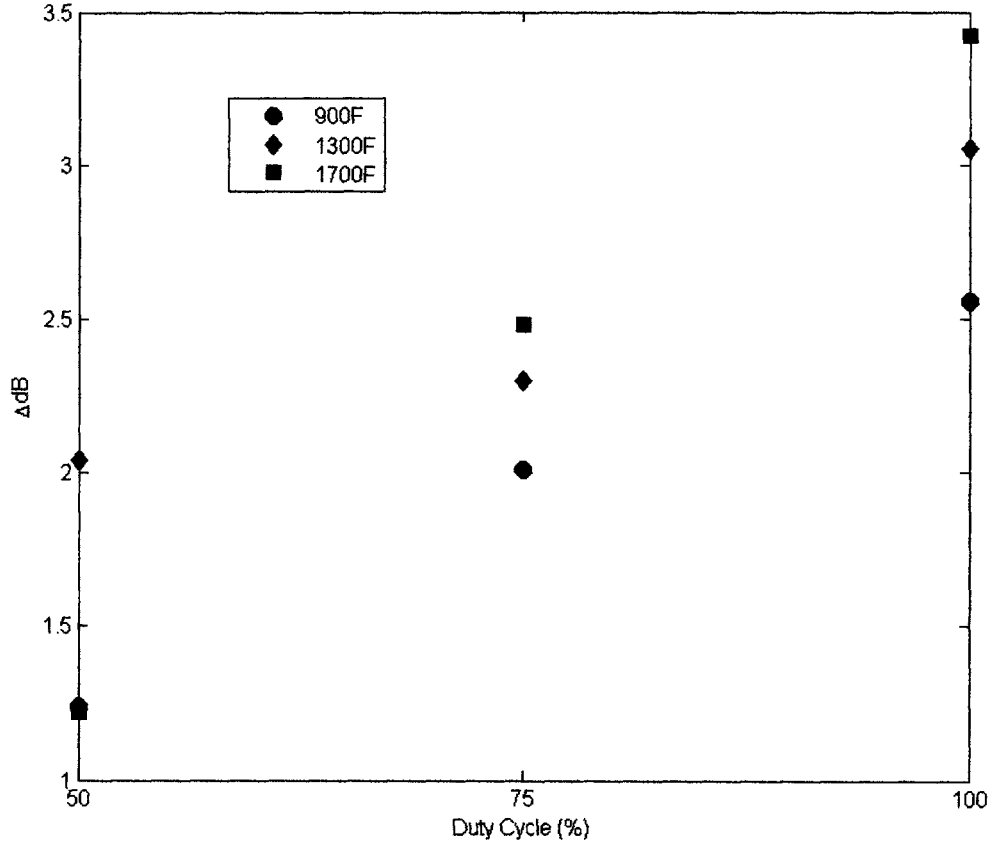
Figure 4.4.6: Noise reduction in the peak radiation direction as a function of duty cycle. Microjets were fired at a pressure of 800 psi. The frequency that produced the greatest reduction in each case was chosen and plotted.

4.5 Frequency Spectra

In order to determine why pulsed microjets are effective at reducing the noise produced by a Mach 1.8 jet, it is necessary to determine what effect they have on the noise-producing mechanisms. The OASPL values calculated and presented in the previous sections are the best indicators of the magnitude of the noise generated by the jet at each operating condition. However, it is necessary to look at the frequency spectra when information about the noise reduction mechanism is desired. As stated previously, Mach wave radiation represents only a small sliver of the high-frequency region of the spectrum. Since the jets in this study were all run at design condition, the remaining spectrum is composed of mixing noise. Therefore, by looking at the spectra, one can determine weather the Mach wave radiation or the mixing noise is reduced.

56

Figure 4.5.1 shows the frequency spectra for the Mach 1.8 jet operating at 900°F for pulsing parameters of (a) 5 Hz and 50% duty cycle and (b) 10 Hz and 75% duty cycle. This figure shows that there is a constant reduction across all frequencies in both cases. Figure 4.5.2 shows the frequency spectra for the Mach 1.8 jet operating at 1300°F for pulsing parameters of (a) 1 Hz and 50% duty cycle and (b) 5 Hz and 75% duty cycle. As for the 900°F jet, constant reductions are seen across all frequencies. The same type of constant reduction across all frequencies is seen in Figure 4.5.3, which shows the frequency spectra for the Mach 1.8 jet operating at 1700°F. Here, the pulsing parameters of (a) 1 Hz and 50% duty cycle and (b) 10 Hz and 75% duty cycle are presented. The particular pulsing parameters for each figure were chosen based on which pair gave the most reduction. All spectra correspond to the noise in the peak radiation direction.

The spectra presented here demonstrate that the reductions for steady and pulsed microjet injection occur over all frequencies. This would imply that pulsed and steady microjet injection is effective in reducing the noise generated by both broadband mixing noise and high-frequency Mach wave radiation.
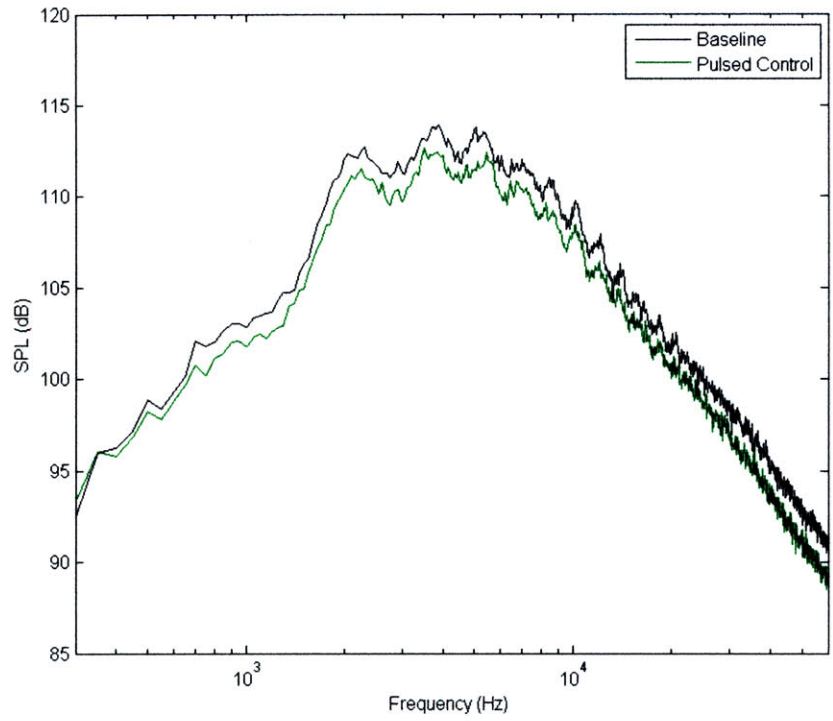
(a)
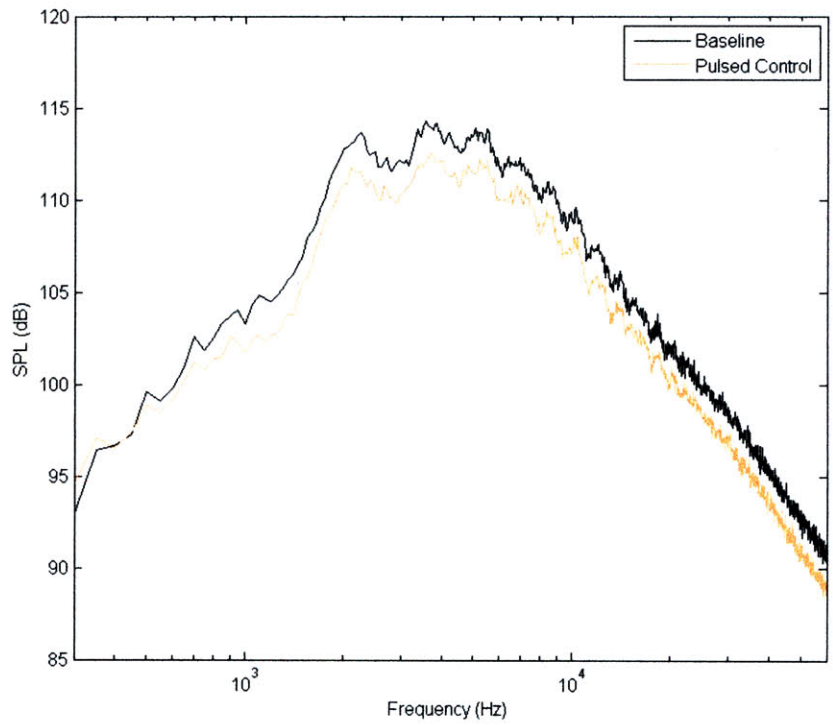
(b)

Figure 4.5.1: Frequency spectra for a Mach 1.8 jet operating at 900°F with pulsing parameters of (a) 5 Hz and 50% duty cycle and (b) 10 Hz and 75% duty cycle.

(a)

(b)

Figure 4.5.2: Frequency spectra for a Mach 1.8 jet operating at 1300°F with pulsing parameters of (a) 1 Hz and 50% duty cycle and (b) 5 Hz and 75% duty cycle.
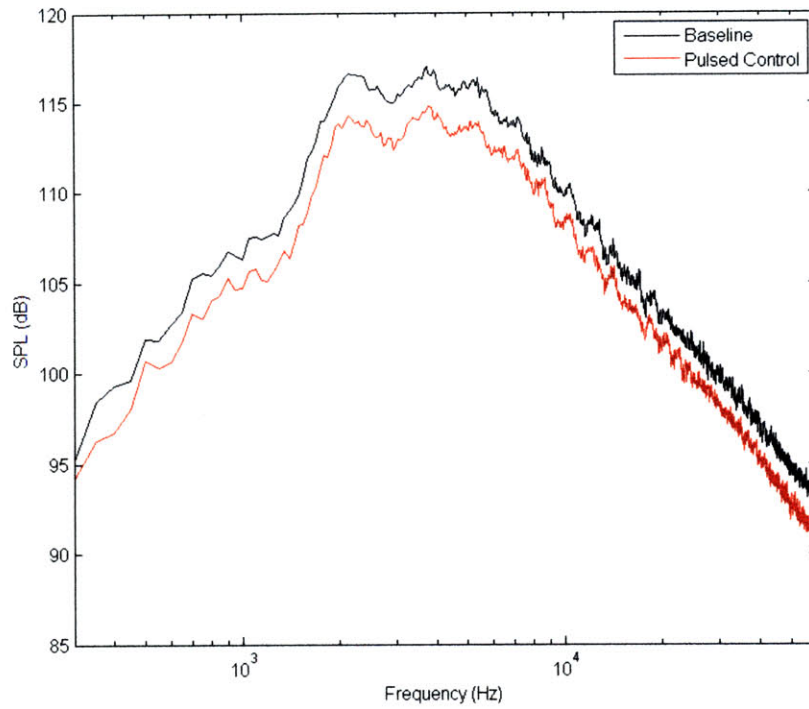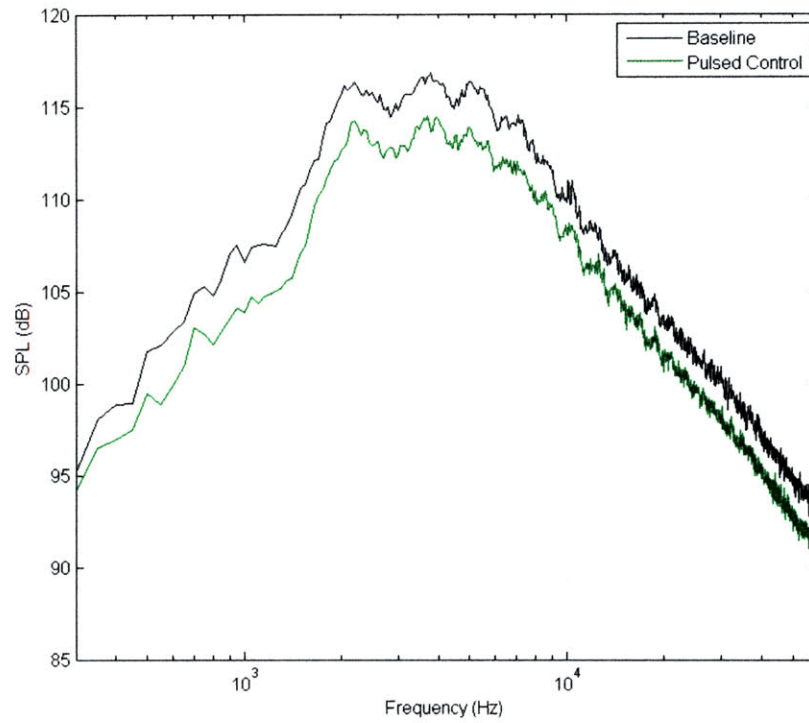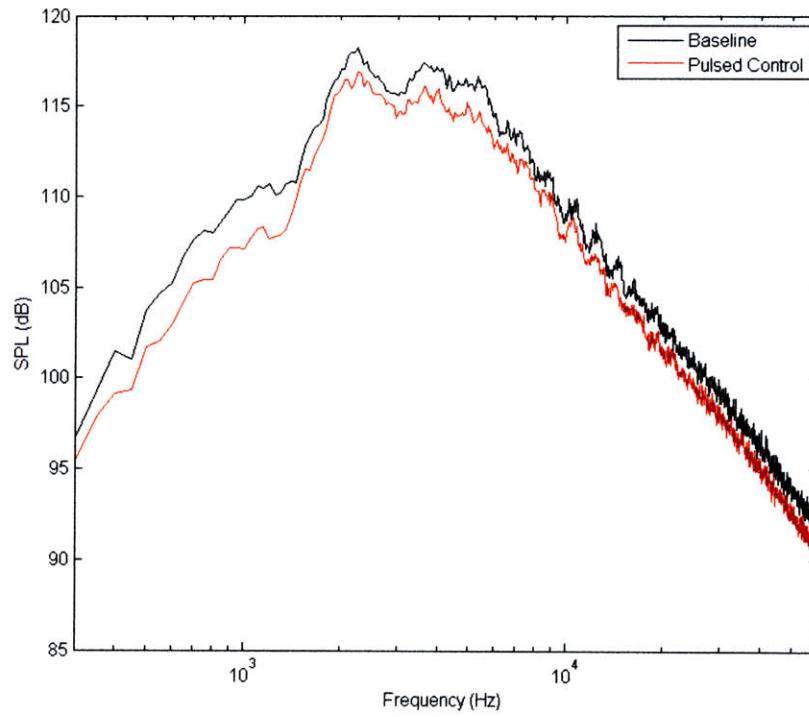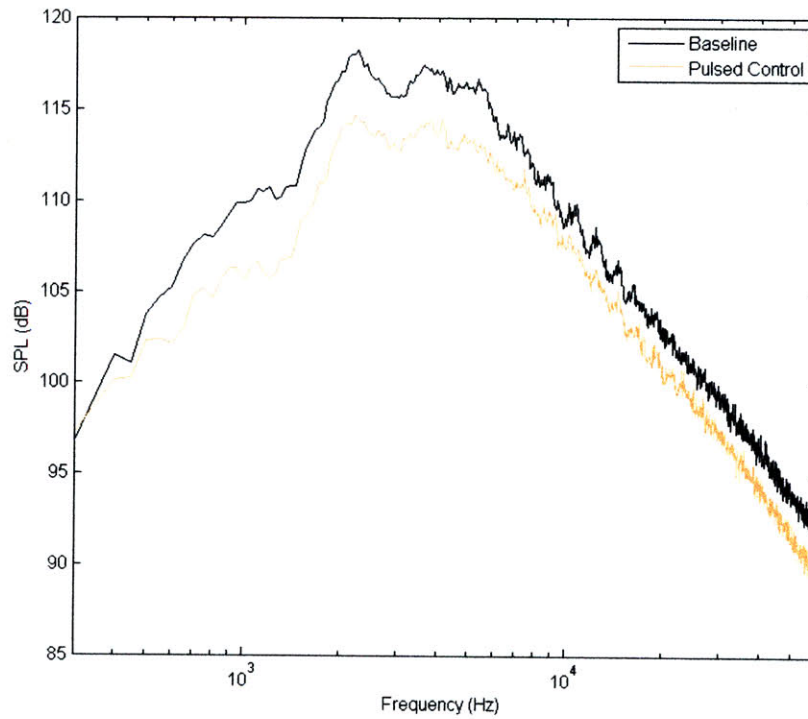
(a)

(b)

Figure 4.5.3: Frequency spectra for a Mach 1.8 jet operating at 1700°F with pulsing parameters of (a) 1 Hz and 50% duty cycle and (b) 10 Hz and 75% duty cycle.

So far the data have been presented in a fashion that compares spectra and OASPL values for injection at the same pressure. However, Figure 4.5.4 shows the spectra for a Mach 1.8 jet operating at 900°F with injection at constant pressure and constant flow rate. At constant pressure, it can be seen from the spectra that pulsing produces a favorable noise reduction. This reduction, however, is not as much as the reduction achieved with steady injection at the same pressure. At constant flow, it is clear from the graph that the reduction achieved with pulsing is comparable with the reduction achieved with steady injection. For some frequencies the reduction associated with pulsed injection surpasses the noise reduction associated with steady injection.

In Figure 4.5.5, the spectra for a Mach 1.8 jet operating at 1300°F at constant pressure and constant flow rate are plotted. Similar to the 900°F case, a favorable noise reduction is achieved using pulsed microjet injection. However, this is not as much as the reduction achieved with steady injection at the same pressure. Also similar to the 900°F case is the fact that the reduction achieved with pulsing is comparable to that achieved with steady injection at a similar mass flow rate.

Figure 4.5.6 shows the spectra for a Mach 1.8 jet at 1700°F at constant pressure and constant flow rate. Again, for a given pressure, the noise reduction achieved with pulsed injection is not as much as the reduction achieved with steady injection. However, the advantage of using pulsing is clearest in this case. For a given flow rate, the noise reduction achieved with pulsing is greater than that achieved with steady injection. This is true for frequencies above 2000 Hz.

In all of these graphs, the reductions are present across all frequencies. This suggesting that pulsed and steady injection reduce both the Mach wave radiation and mixing noise mechanisms. It should be noted that through pulsing, energy is introduced into the system at low frequencies. The data below frequencies of 300 Hz is not shown because the anechoic chamber is only rated down to that frequency. Any measurements obtained below 300 Hz cannot be taken as good measurements. However, the spectra do show an increase in the energy at low frequencies. While this is most likely due to the mechanism of pulsing, the energy increase is only over a small frequency band (less than 300 Hz) as compared with the presented frequency band (300 Hz to 60,000 Hz), and therefore does not contribute significantly to the overall sound pressure level.
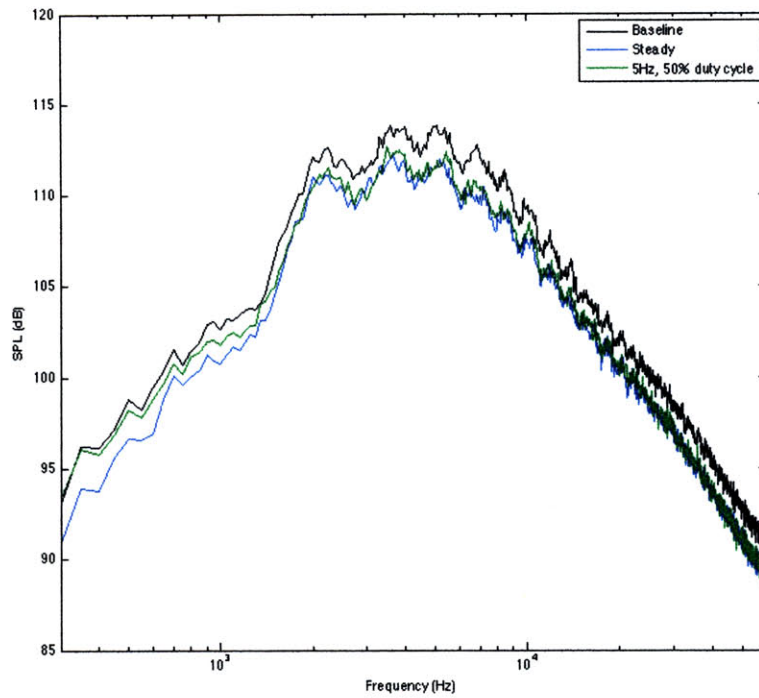
(a)
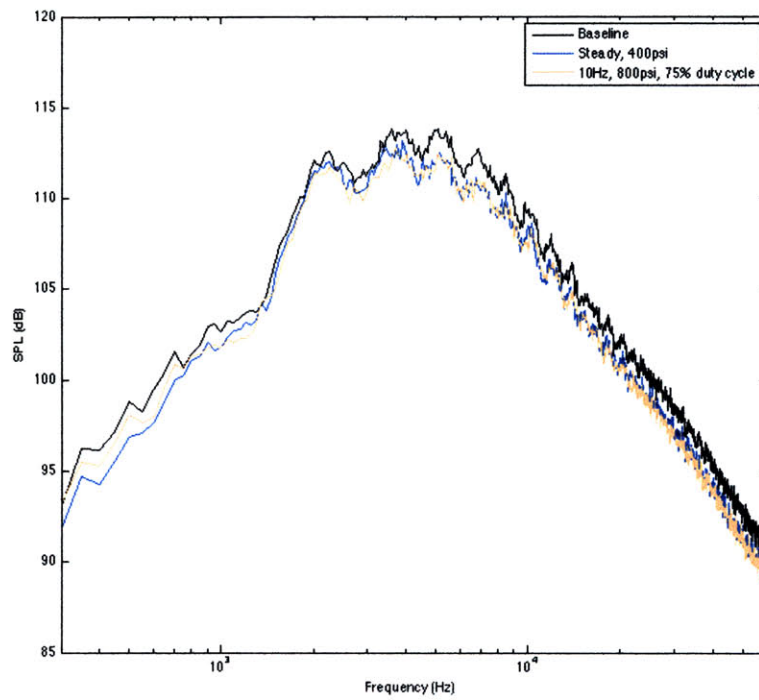
(b)

Figure 4.5.4: Spectra for a Mach 1.8 jet operating at 900°F with injection at (a) constant pressure and (b) constant flow rate.
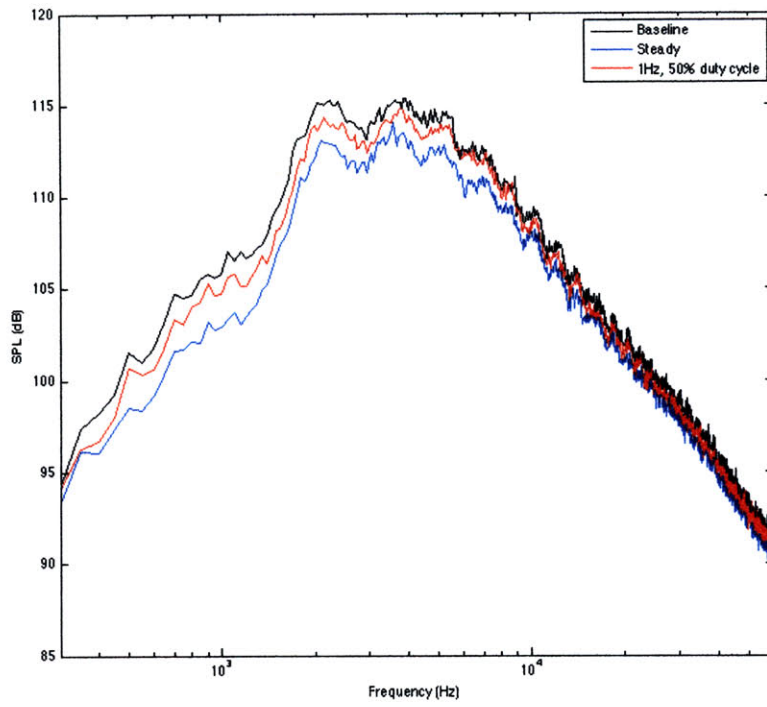
(a)
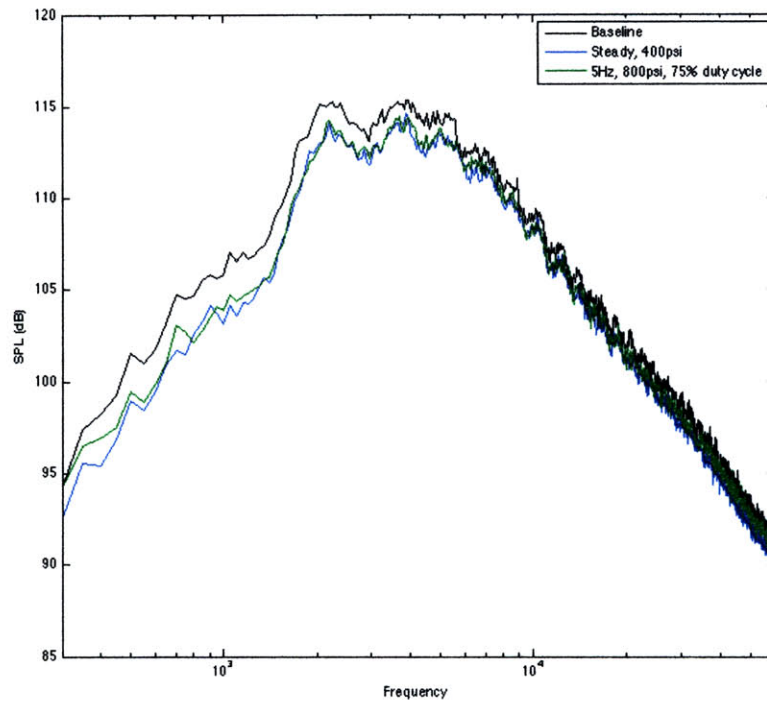
(b)

Figure 4.5.5: Spectra for a Mach 1.8 jet operating at 1300°F with injection at (a) constant pressure and (b) constant flow rate.
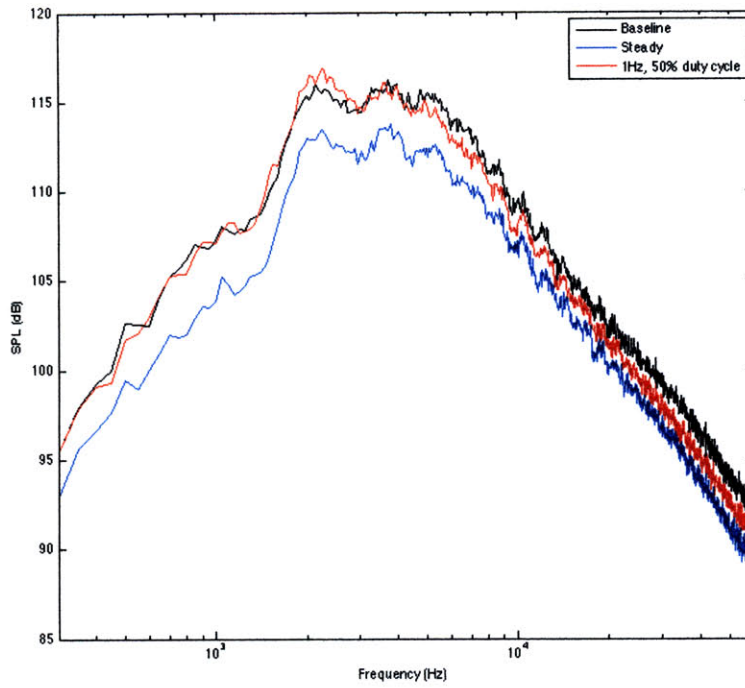
(a)
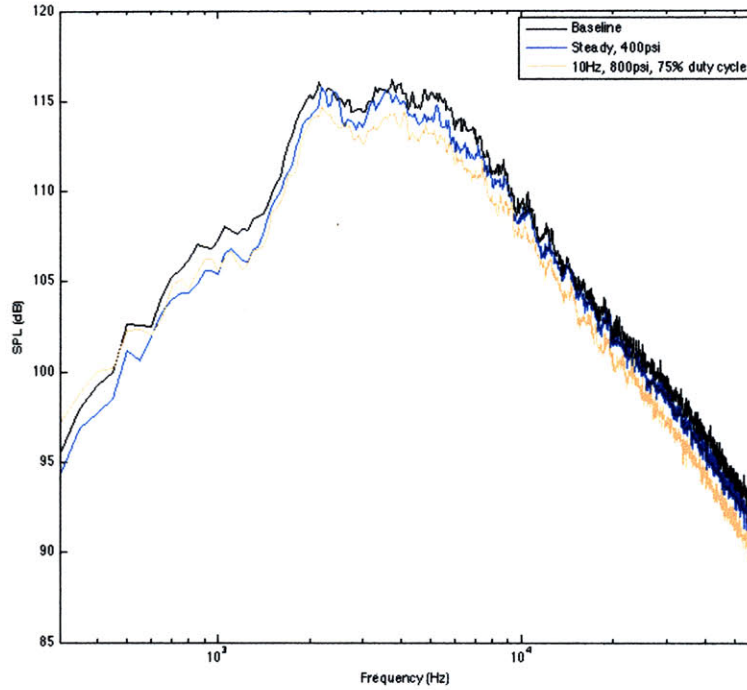
(b)

Figure 4.5.6: Spectra for a Mach 1.8 jet operating at 1700°F with injection at (a) constant pressure and (b) constant flow rate.

4.6 Observations

Previous work has demonstrated that the noise generated by a supersonic jet could be reduced significantly through the use of steady, aqueous microjet injection. Practically speaking, aqueous microjet injection, though effective as it is, represents a serious complication in that the weight of the fluid required makes its use prohibitive. The primary goal of this research, therefore, was to determine whether those same noise reductions could be achieved with less water usage.

The initial results suggest several trends. One would expect that reducing the amount of water would also reduce the efficacy of the microjet. This is true only to an extent. We can see that though pulsed microjets do not stand up to their steady counterpart at the same pressure, they prove to be more effective when compared to steady injection at the same mass flow rate. With respect to the experiments presented herein this fact is true across the board, in all cases. It should be noted that there is a discrepancy between the steady microjet injection noise reduction obtained in this study versus that obtained by Greska [12]. This is due to the fact that at a given pressure, less water flows through the fuel injectors than through the simple tube microjets used by Greska. This is due the larger pressure drop that results from the flow around the plunger and through the tip.

To summarize, the OASPL is plotted as a function of exhaust temperature for a Mach 1.8 jet in figure 4.6.1. The points are connected to show trend only, and do not serve to suggest a function of any kind. For constant pressure injection, steady is clearly the best. Only slightly less effective is pulsed injection at a duty cycle of 75%. Pulsed injection at 50% duty cycle is the least effective. For constant flow rate, however, pulsing is more effective than steady injection for all of the exhaust temperatures tested. Pulsed injection at 50% duty cycle is not plotted here because the flow rate does not compare to steady injection at any pressure.
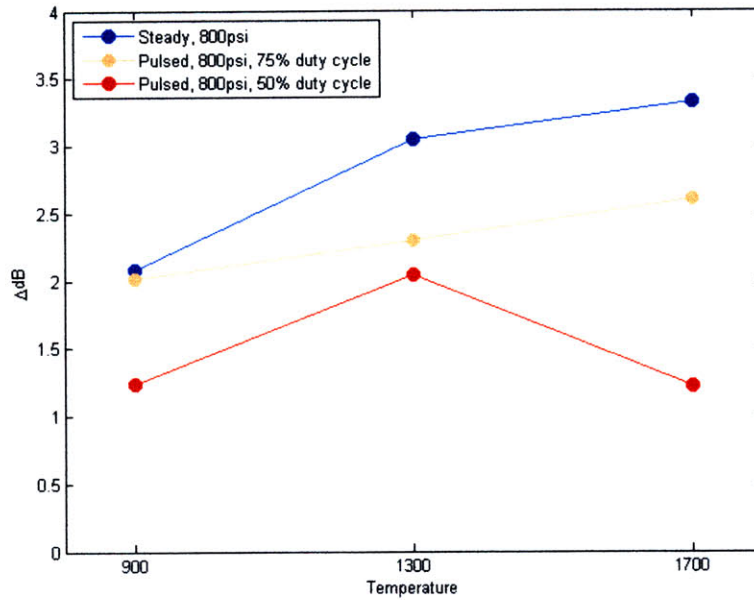
(a)
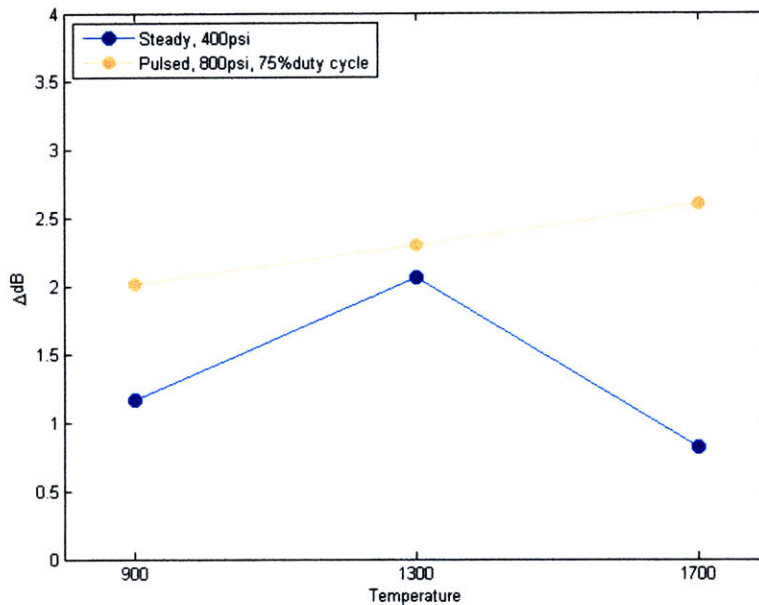
(b)

Figure 4.6.1: OASPL as a function of temperature for microjet injection at (a) constant pressure and (b) constant flow rate.

We have found that Mach 1.8 jet noise reduction can be achieved with similar success to noise reductions from steady microjet injection, but with less water used. However, many new questions have arisen. Clearly, the efficacy of the pulsed microjets is a function of several variables that were not tested within the scope of the research

66

presented in this thesis. Pulsed microjet operation may be varied by changing its frequency and duty cycle. However, as seen from the results thus far, the optimal frequency and duty cycle pair still requires further investigation. The optimum parameters are clearly affected by temperature, as seen by the data, but presumably by jet Mach number as well. A way to perhaps extract the optimum values for these parameters is discussed in the following chapter. Additionally, steady injection holds one key advantage over pulsed microjet injection: the flow during steady injection is constant, whereas the flow through a pulsing injector is constantly changing. When the plunger of the valve is closed, it physically blocks the flow of water through the exit. However, when it is opened, water must overcome its inertia and begin moving around the plunger and through the opening. Therefore, the velocity profile of the pulsed jets may not be as ideally square-wave as we would hope, as in Figure 4.6.2. This is a function of water's density and viscosity. Using an alternate fluid with different properties would, presumably, change this.
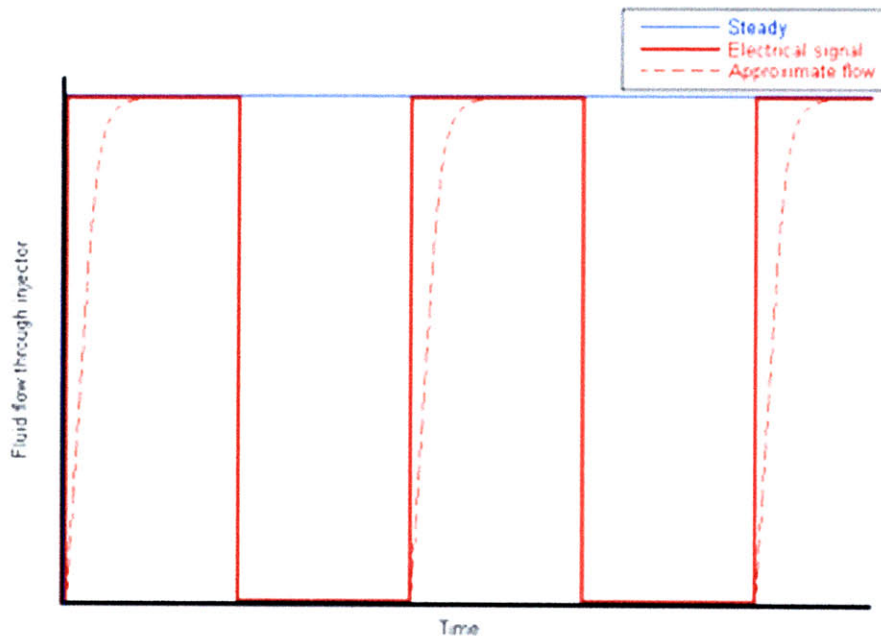
Figure 4.6.2: Control signals generated by steady injection (blue), electrical signal sent to the injectors (solid red) and the approximate flow output (dotted red).

CHAPTER 5

CONCLUSIONS AND FUTURE STUDY

5.1 Conclusions

The first undeniable conclusion at which one arrives from Chapter 4 is that pulsing accomplishes the same noise reduction as steady injection while using less water. The only exception to this conclusion is the data presented in Figure 4.6.1 (a) which may lead one to conclude that noise reductions greater than 2.8 dB cannot be realized with pulsing but only with steady injection (for temperatures of 1300 and 1700°F). It is argued below that this is not necessarily the case.

The data presented in Figure 4.3.2 are shown again in Figure 5.1.1. From Figure 4.3.2, nine data points obtained at the three temperatures are presented, along with 3 projected data points. The first data point corresponds to steady injection at 400 psi, and is given a blue open symbol. The second corresponds to steady injection at 800 psi, and is given a blue closed symbol. A closed red, green or orange symbol corresponds to pulsing at 800 psi at a frequency of 1, 5 or 10 Hz, respectively. The last point shows the projected noise reduction that may be achievable at a much higher injection pressure ofr pulsing. This is marked with an open star-shaped symbol. These additional points show that higher noise reductions than those shown in Figure 4.3.2 may be achieved with pulsing by injecting at pressures that are higher than 800 psi. They also show that this reduction would correspond, as in the case with the 1.2 dB reduction, to smaller water consumption. To achieve these data points, a pressure of 2175 psi would be required in the 900°F case, while 2290 psi would be required in the 1300 and 1700°F cases. This has

not been tested experimentally, as yet, as the pressures exceed the limits of the current water supply network.
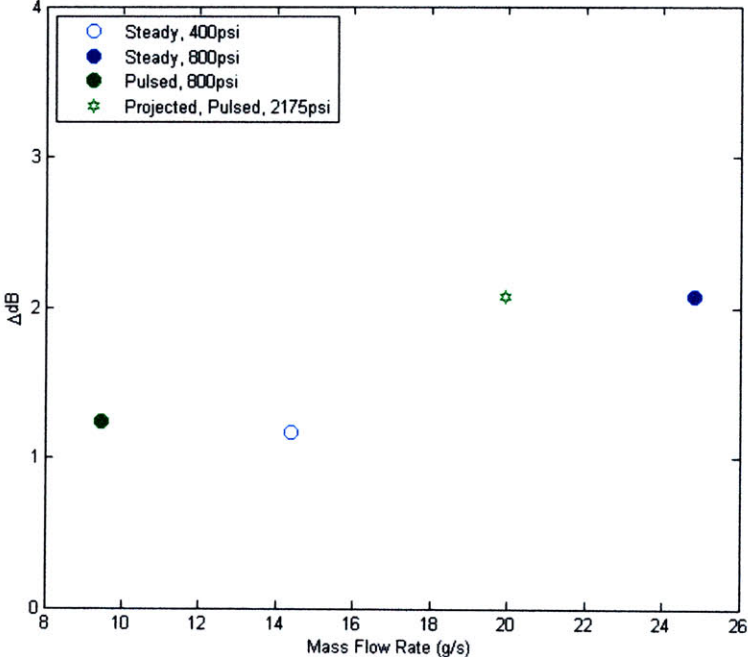
(a) 900°F
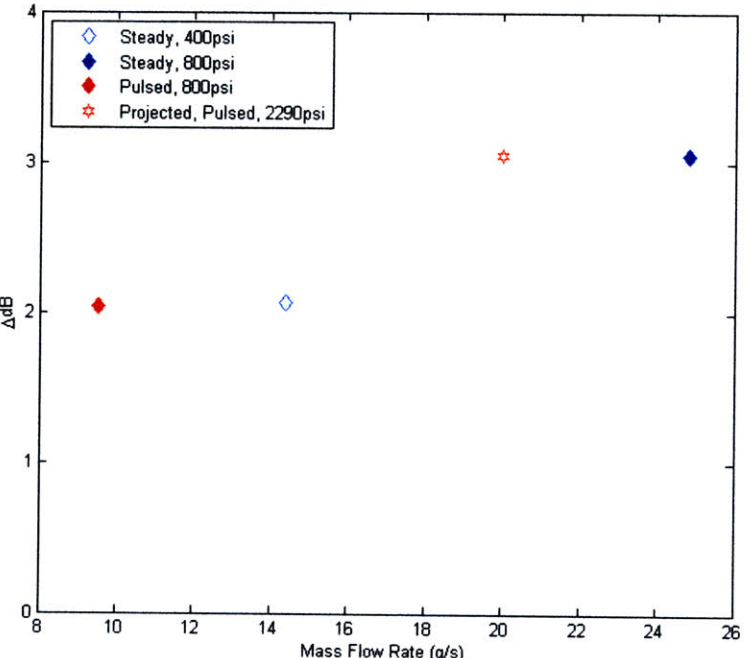
(b) 1300°F
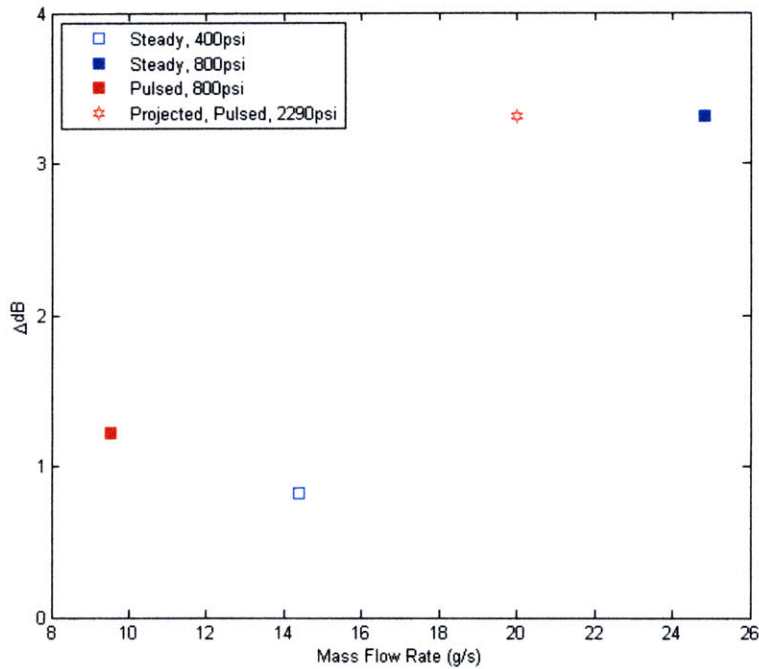
(c) 1700°F

Figure 5.1.1: Achieved and projected noise reduction as a function of mass flow rate through each injector for a jet at (a) 900°F, (b) 1300°F and (c) 1700°F.

Several advantageous pulsing configurations have been discovered. For a Mach 1.8 jet operating at 1700°F, 90.2% of the steady injection noise reduction is achieved with 46% of the water used when pulsing at 5 Hz with a pressure of 400 psi and a duty cycle of 50%. At 1300°F, 66.9% of the steady injection noise reduction is achieved with 38.4% of the water used when pulsing at 1 Hz with a pressure of 800 psi and a duty cycle of 50%. Also, at 900°F, 85.3% of the steady injection noise reduction is achieved with 54% of the mass flow rate used at 10 Hz with a pressure of 800 psi and a duty cycle of 50%. These configurations demonstrate comparable noise reduction with significantly less water used.

In testing the hypothesis, several other key discoveries were made. First, it was found that in varying the duty cycle of the pulsing, the noise suppression could be increased. Increasing the duty cycle (in this study from 50% to 75%) increases the total noise reduction. There also appears to be a parabolic trend in the noise reduction as a function of duty cycle. This suggests that there exists an optimum duty cycle at which the noise reduction is the greatest for a given mass flow rate.

71

The frequency spectra for steady and pulsed microjet injection show reduced noise over all of the frequencies studied. This suggests that microjet injection reduces both the Mach wave radiation, which inhabits the high-frequency range of the spectra, as well as broadband mixing noise, which is composed of all frequencies.

5.2 Transient Effects and System Identification

Logically, flow characteristics of, and therefore the noise generated by, a supersonic jet will not change instantaneously in response to an external flow source. Rather, there will be some short time period immediately following the initiation of control in which the jet will respond continuously with a given behavior. Likewise, upon termination of external control, the jet may return to its baseline condition continuously over a different short time period with an associated behavior. The behavior and timescales of these transient phenomena are unknown and presumably dependent on the run condition. A sample transient behavior is presented in Figure 5.2.1. In conjecture, certain behaviors could prove advantageous, and could render an increased noise reduction provided that the proper time constants are extracted from the behavior of the jet during transient periods. For example, in Figure 5.2.1, the microjets are turned on at time t_0. After a brief delay lasting t_1-t_0, the initial free jet response is seen and lasts t_2-t_1. The steady-state behavior is seen therefore after time t_2. It was necessary to perform a series of experiments designed to enable the extraction of these time constants for the purpose of determining the optimum pulsing characteristics.
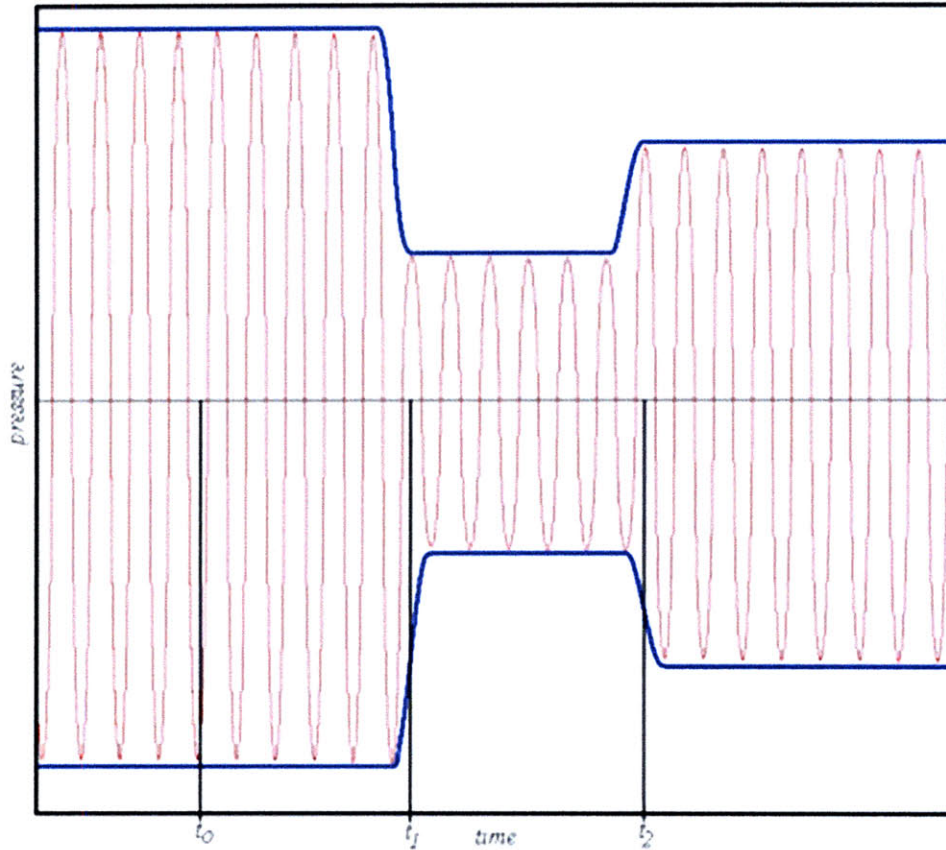
Figure 5.2.1: Simplified potential time response of the jet dynamics.

An experiment in which the jet noise output may be matched exactly with the control input would be ideal. With respect to control theory, this would produce a set of data essentially composed of a series of input-output pairs of the form [u(t),p(t)]. In this case, the input is the microjet injection. It is composed of a square wave with a value that is either zero or one. Zero corresponds to microjets off, and one corresponds to microjets on. The pressure-time signal is the output. A simple block diagram of this concept is shown in Figure 5.2.2. Though unknown, given the input and output pairs, the jet response transfer function, T(s), may be determined. Theoretically, this allows for the establishment of an ideal input given the derived transfer function and a desired output. That is,

$$U(s) = \frac{P(s)}{T(s)}.$$

P(s) and U(s) are the Laplace transformed pressure and control input equations, p(t) and u(t), respectively. In this case, U(s) is the Laplace transformed ideal control input. The

73

results of these tests, as well as establishment of a system transfer function, will allow the "sweet spot" with respect to frequency and duty cycle to be found.
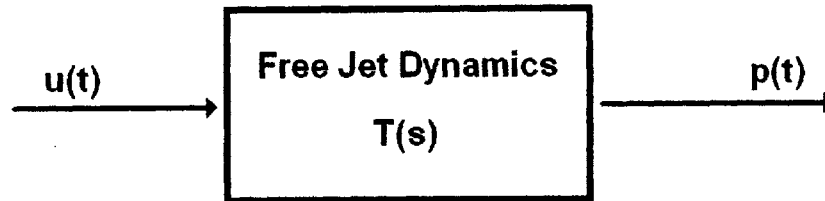
Figure 5.2.2: Simple block diagram of the free jet dynamics with pulsed microjet control input and pressure signal output.

Several of these transient tests have been conducted so far, mainly on a Mach 1.5 jet. Figure 5.3.3 shows the transient behavior for a Mach 1.5 jet at (a) 900°F, (b) 1300°F and (c) 1700°F jet. The behavior of the jet is extremely erratic, which makes trendspotting quite difficult. For this reason, the pressure-time signal was integrated and normalized to better show the effects of the microjet stimulus. Therefore, any point in

the curve may be found by $\bar{p}_i = \dfrac{\sum\limits_{j=1}^{i} p_j^2}{\sum\limits_{k=1}^{N} p_k^2}$, where N is the total number of samples in the set,

or 1,433,600 in this case. Basically, the slope of the curve represents the magnitude of the pressure-time signal at that instant.

Looking at Figure 5.2.3a, the baseline pressure signal of the Mach 1.5 jet at 900°F can be seen from time equal to 1.02 s to about 1.06s. It should be noted that the microjets were turned on at time equal to 1.00 s exactly. There is, of course, a simple time delay that arises as a result of the time it takes for the jet to respond, as well as the time required for the pressure signals originating at the nozzle exit to reach the microphones and data acquisition cards. From there, the slope of the pressure signal drops significantly from 1.06 s to about 1.08 s. After that point, the noise settles into its steady-

state value associated with steady microjet injection. One detail to be noticed is the fact that the slope during the middle transient region is less than the slope during the steady-state microjet injection region. This suggests that there is about a 0.02 s time period when the jet is responding to the flow control, during which the noise level is below that of steady state. Given this, it could be suggested that an optimum frequency for noise suppression would be commensurate with this particular time constant.

Figure 5.2.3b shows the integrated pressure signal for a Mach 1.5 jet operating at 1300°F. The baseline pressure signal can be seen from the onset to about time equal to 1.04 s. From there, the slope drops dramatically from time equal to 1.04 s to 1.05 s. Then, as before, the slope settles into its steady-state value associated with steady microjet injection. In this case, the period of time during which additional noise suppression is achieved is about half that of the 900°F case. This demonstrates the effect temperature has on the optimal pulsing frequency.

Further demonstrating this point is Figure 5.2.3c. For this case, where the Mach 1.5 jet is operating at 1700°F, the changes in slope are more ambiguous. However, it can be seen that the added noise suppression region is even shorter, lasting only from about time equal to 1.045 s to 1.05 s. While these results are limited in their scope, they show clearly that the temperature of the jet affects the optimum pulsing frequency.

(a)

(b)

76
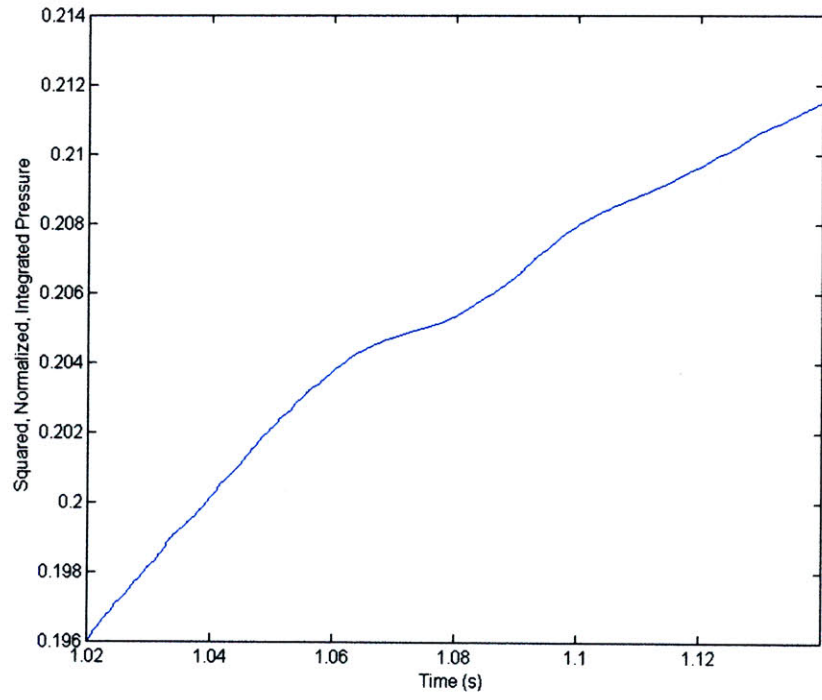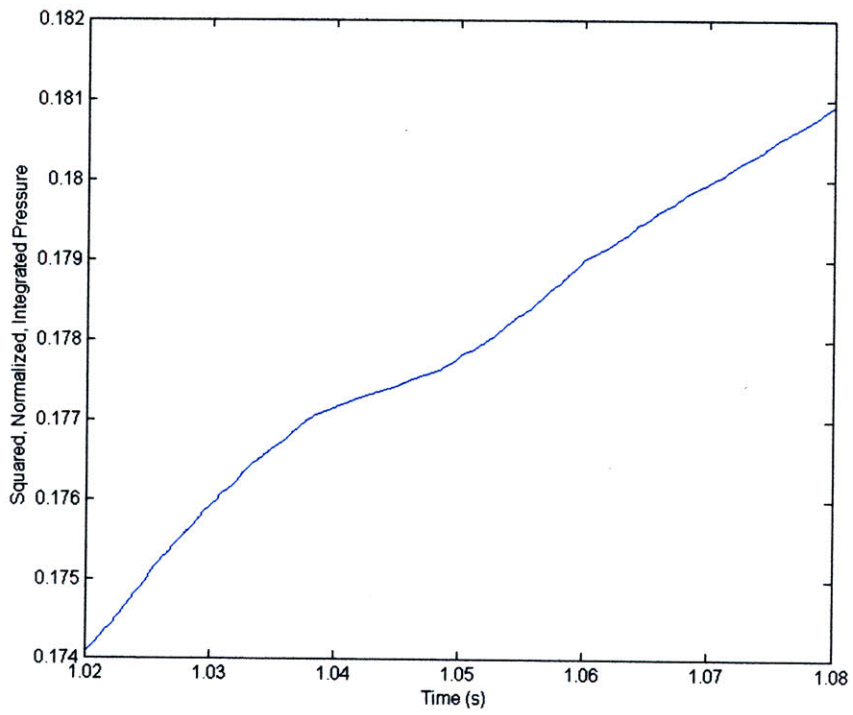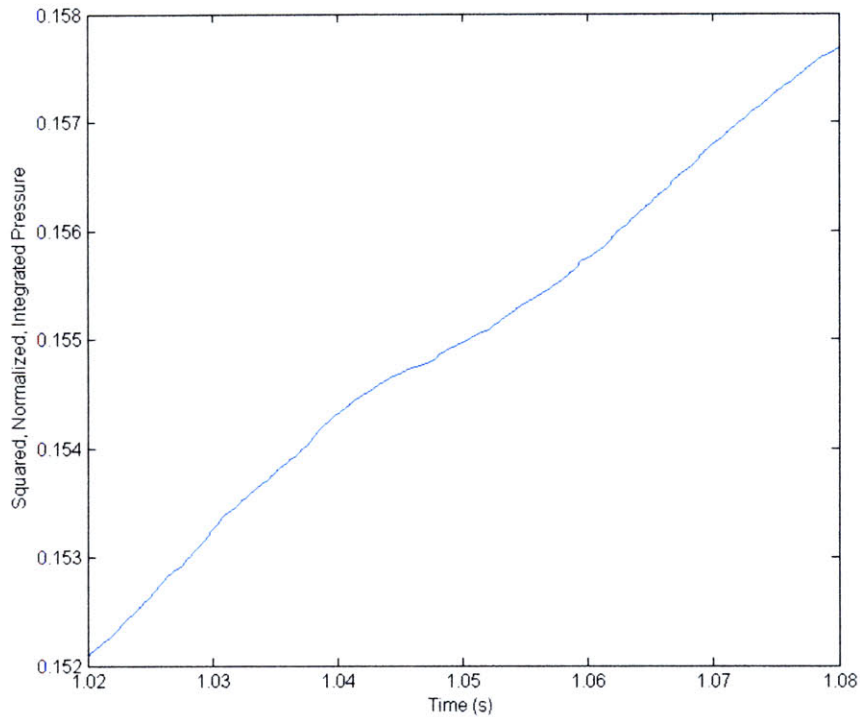
(c)

Figure 5.2.3: Transient behavior of the pressure signal generated by a Mach 1.5 jet operating at (a) 900°F, (b) 1300°F, and (c) 1700°F. The signal has been squared, normalized, and integrated for clarity.

It is apparent from all three parts of Figure 5.2.3 that there is a period immediately after the initiation of control in which the noise produced by the jet drops below that generated during steady-state. The mechanism that causes this behavior is currently unknown, though it is believed to be a result of the initial impingement of the fluid microjets into the main jet. This initial fluid impingement interacts with the shear layer, in a transient form, until the steady-state fluid stream develops. This initial interaction could be responsible for the additional reduction seen during that short time period. It appears to be a property of the jet, since the behavior is repeatable, and is a function of temperature and, presumably, Mach number.

5.3 Future Study

The work presented in this thesis only scrapes the surface of the investigation of pulsed microjet injection as a means of supersonic jet noise suppression. Clearly it has

been demonstrated that for a Mach 1.8 jet operating ideally at various temperatures, the noise reduction obtained using steady microjet injection may be sustained using less water when the microjets are pulsed at relatively low frequencies. However, as a result of the findings of this work, it becomes apparent that the ultimate goal of this research is to determine the optimum pulsing characteristics that will produce the greatest noise reduction using the least amount of fluid.

The first step in this process is to continue transient testing. Since jet temperature and potentially Mach number affect the pulsing parameters, these tests must be performed for other Mach numbers. The tests have been performed for Mach 1.5, but will be performed for Mach 2.0, 1.8, 1.3, sonic and subsonic conditions. For each condition, a period of time will be determined that corresponds to the duration of the added noise suppression region of the transient integral plot. This gives the length of time the injectors can stay on before the jet adapts to its steady-state condition. When the microjets are turned off, the noise will return to the baseline value. The length of time it takes to do so will correspond to the maximum length of time the microjets may remain off. The inverse of the sum of these two time constants will give the pulsing frequency, while the ratio of the first time constant to the sum of the two will give the duty cycle. That is,

$$f_{pulse} = \frac{1}{T_{reduction} + T_{rise}}$$

and

$$duty\ cycle = 100 \times \frac{T_{reduction}}{T_{reduction} + T_{rise}}.$$

These found parameters would need to be tested experimentally, though they show promise in their ability to meld classic fluid mechanics with controls engineering.

A rough determination of the optimal pulsing frequency for a Mach 1.5, 900°F jet was derived from Figure 5.2.3a. The period of additional noise reduction, which last approximately 20 ms, corresponds to a pulsing frequency of 50 Hz. However, when pulsed control was employed for those operating conditions, the jet became excited and a tone was produced. This tone was not present while testing the microjets at the same frequency while the jet was off. This suggests that the tone generated was not a result of

78

structural resonance, but rather a result of some fluid mechanical process within the jet itself. In this work, only 1, 5, and 10 Hz pulsing frequencies were tested. However, future work will involve testing more frequencies and duty cycles around the 50 Hz range.

So far, all the work described involves pulsing each injector at the same time. Simultaneous voltage signals are sent to the injectors so that they open and close synchronously. However, the driver used to control the injectors is capable of firing each individually, or in stages of two or three. This opens another pulsing parameter: spatial order. It may be more effective to pulse the injectors in a certain order, rather than simultaneously. This will need to be tested experimentally as well.

And finally, to ensure that larger reductions are possible than those presented here, injection at higher supply pressure will need to be tested.

These tests are all designed to determine whether optimum pulsing parameters exist. Without providing an answer as to why the process is effective leaves the solution incomplete. Therefore, flow visualization of some sort will be performed. Either a Schlieren or shadowgraph technique will be used to determine the actual flow dynamics of the jet under the influence of pulsed microjet control.

APPENDIX A

OASPL Values

OASPL Values for a Mach 1.8, Ideally Expanded Jet at 900°F with 800 psi Injection at 50% Duty Cycle

Angle	Baseline	Steady	1Hz	5Hz	10Hz
150	134.0145	132.9779	133.5010	133.1545	133.9763
145	135.2489	133.8599	134.4633	134.3561	134.9039
140	135.9242	134.6245	135.2094	134.9486	135.7442
135	136.6773	134.5988	135.5933	135.4380	136.2216
130	136.3698	134.1137	135.3151	135.0246	135.6602
125	133.3905	132.2961	133.0213	132.3217	133.2599
120	128.9118	128.9362	129.1498	128.6727	129.3225
115	126.3657	126.5537	126.6951	126.4655	126.7619
110	124.4312	124.4995	124.6649	124.7315	124.8274
100	121.6676	122.1072	121.9295	121.9733	122.3140
90	120.3410	120.3990	120.4684	120.4923	120.5114
80	118.6673	118.9755	118.9410	119.1508	119.0165

OASPL Values for a Mach 1.8, Ideally Expanded Jet at 1300°F with 800 psi Injection at 50% Duty Cycle

Angle	Baseline	Steady	1Hz	5Hz	10Hz
150	135.6162	133.7855	134.1758	133.9191	134.5121
145	136.4828	134.8521	135.4063	135.1004	135.4975
140	137.5468	135.5550	136.1885	136.0866	136.4739
135	138.3741	135.8755	136.8098	136.7538	137.3278
130	138.8165	135.7654	136.7766	136.8553	137.5886
125	137.3681	134.9787	136.1929	135.8997	136.8814
120	133.7472	131.9938	132.8112	132.6676	133.5922
115	129.9690	129.5009	129.2868	129.2395	129.8089
110	127.9027	127.3702	127.2812	127.0079	127.4714
100	124.7971	123.9302	124.4120	124.3503	124.8400
90	122.7721	122.5269	122.0147	122.7805	122.6926
80	121.0910	121.1488	120.8532	120.9601	120.7778

OASPL Values for a Mach 1.8, Ideally Expanded Jet at 1700°F with 800 psi Injection at 50% Duty Cycle

Angle	Baseline	Steady	1Hz	5Hz	10Hz
150	134.4623	133.5990	134.2756	134.9805	134.2200
145	135.7092	134.4768	134.9132	136.0275	135.2262
140	136.9753	135.0606	136.4079	136.4314	136.6360
135	138.1916	135.4184	137.5827	137.3945	137.3721
130	138.7643	135.4557	137.5417	137.6840	137.5923
125	138.2041	134.9271	137.0058	137.0528	137.6746
120	135.3557	132.8898	134.4950	133.9507	135.6517
115	131.3270	129.8249	130.7341	130.7518	132.0352
110	128.7157	127.1643	128.0963	128.1139	129.2116
100	124.8733	123.4458	124.7130	124.1483	125.0312
90	122.4208	122.0375	123.2370	122.6716	123.0749
80	120.5321	120.3453	121.5338	120.9701	121.6324

OASPL Values for a Mach 1.8, Ideally Expanded Jet at 900°F with 400 psi Injection at 50% Duty Cycle

Angle	Baseline	Steady	1Hz	5Hz	10Hz
150	133.6052	133.6207	134.0581	133.4200	133.8396
145	134.9055	134.5392	135.1431	134.4586	134.9402
140	135.6722	135.2865	135.9869	135.2056	135.7487
135	136.3895	135.6324	136.3479	136.0190	136.3103
130	136.5028	135.3356	136.0673	136.0659	135.9554
125	133.7694	133.8515	133.1861	133.8783	133.7581
120	129.1675	130.6109	129.3436	129.7984	129.1973
115	126.7486	127.5367	127.0522	127.1516	126.8858
110	125.2811	125.5295	125.4550	125.4154	125.0834
100	122.6856	122.8650	122.3482	122.3421	122.4946
90	120.6378	120.7859	120.9682	120.8755	120.9964
80	119.5519	119.8201	119.6417	119.6809	119.5476

OASPL Values for a Mach 1.8, Ideally Expanded Jet at 1300°F with 400 psi Injection at 50% Duty Cycle

Angle	Baseline	Steady	1Hz	5Hz	10Hz
150	135.0787	134.6236	134.0496	134.2159	134.9204
145	136.2960	135.2650	135.0387	135.6509	135.8607
140	137.4859	135.9893	135.8970	136.7865	136.3045
135	138.4441	136.3810	136.8383	137.7840	137.1148
130	138.4166	136.2391	136.9850	137.7487	137.4762
125	137.5081	135.5446	136.6822	136.9986	136.2343
120	133.4761	132.6211	133.3816	133.4918	132.3490
115	129.6832	139.1797	129.9953	129.8628	128.9001
110	127.7406	126.8056	127.8649	127.9572	126.3771
100	124.6187	123.9946	124.8874	124.3635	123.6021
90	122.8787	122.0942	122.8324	122.1080	121.6820
80	122.1093	120.6233	120.9831	120.4600	120.8878

OASPL Values for a Mach 1.8, Ideally Expanded Jet at 1700°F with 400 psi Injection at 50% Duty Cycle

Angle	Baseline	Steady	1Hz	5Hz	10Hz
150	134.7339	134.2270	135.0030	134.0902	134.1569
145	135.5183	134.9024	136.0770	135.3197	135.0579
140	136.6144	135.9848	137.0407	136.5566	136.3127
135	137.2166	137.0015	137.7851	137.1849	137.4094
130	138.1123	137.2907	137.9858	137.3711	137.4642
125	137.2550	136.9242	137.6675	137.1333	137.0141
120	134.8733	134.8239	135.1180	134.1621	134.1015
115	130.7121	130.9953	130.9173	130.5787	130.4261
110	128.3226	128.4308	128.4989	128.1477	127.7609
100	125.0785	125.1239	124.4998	125.1393	124.1645
90	122.5802	123.2275	122.6539	122.7376	122.1656
80	121.0910	121.3331	121.1589	121.8179	120.8331

OASPL Values for a Mach 1.8, Ideally Expanded Jet at 900°F with 800 psi Injection at 75% Duty Cycle

Angle	Baseline	Steady	1Hz	5Hz	10Hz
150	134.1737	133.2929	133.8755	133.7666	133.3614
145	135.4618	134.2427	134.7543	134.5627	134.2976
140	136.6149	134.8260	135.2819	135.1415	134.8896
135	137.3017	134.9462	135.6381	135.5700	135.2919
130	136.5963	134.1935	135.1573	135.1862	134.9063
125	133.4789	132.1262	132.7962	132.9208	133.0270
120	129.1996	128.7559	129.3700	129.2365	129.2861
115	127.1308	126.3384	126.7831	126.6917	126.8871
110	125.4221	124.4644	124.7372	124.5314	124.9204
100	122.2784	121.6044	122.1062	122.0857	122.0102
90	120.7232	119.9498	120.1881	120.3610	120.5359
80	119.4879	119.2874	119.0187	119.0556	119.4445

OASPL Values for a Mach 1.8, Ideally Expanded Jet at 1300°F with 800 psi Injection at 75% Duty Cycle

Angle	Baseline	Steady	1Hz	5Hz	10Hz
150	134.8975	134.0461	134.3978	134.2002	134.7030
145	136.2244	134.9713	135.6662	134.8672	135.5671
140	137.3028	135.3380	136.6196	135.8132	136.0128
135	138.6428	135.8325	136.7712	136.5242	136.8940
130	138.7928	135.9413	136.7759	136.4930	136.7225
125	137.5359	135.0840	135.8273	135.2214	135.3475
120	133.6313	132.2751	132.5818	132.1858	132.3044
115	130.1995	129.0233	129.4176	129.4700	129.2426
110	127.7996	126.5521	126.9816	127.4810	126.9705
100	124.7835	123.6222	123.7717	123.9897	123.9790
90	122.8280	122.0225	122.2667	121.7970	122.2291
80	120.9990	121.1203	121.0739	120.3193	120.4033

OASPL Values for a Mach 1.8, Ideally Expanded Jet at 1700°F with 800 psi Injection at 75% Duty Cycle

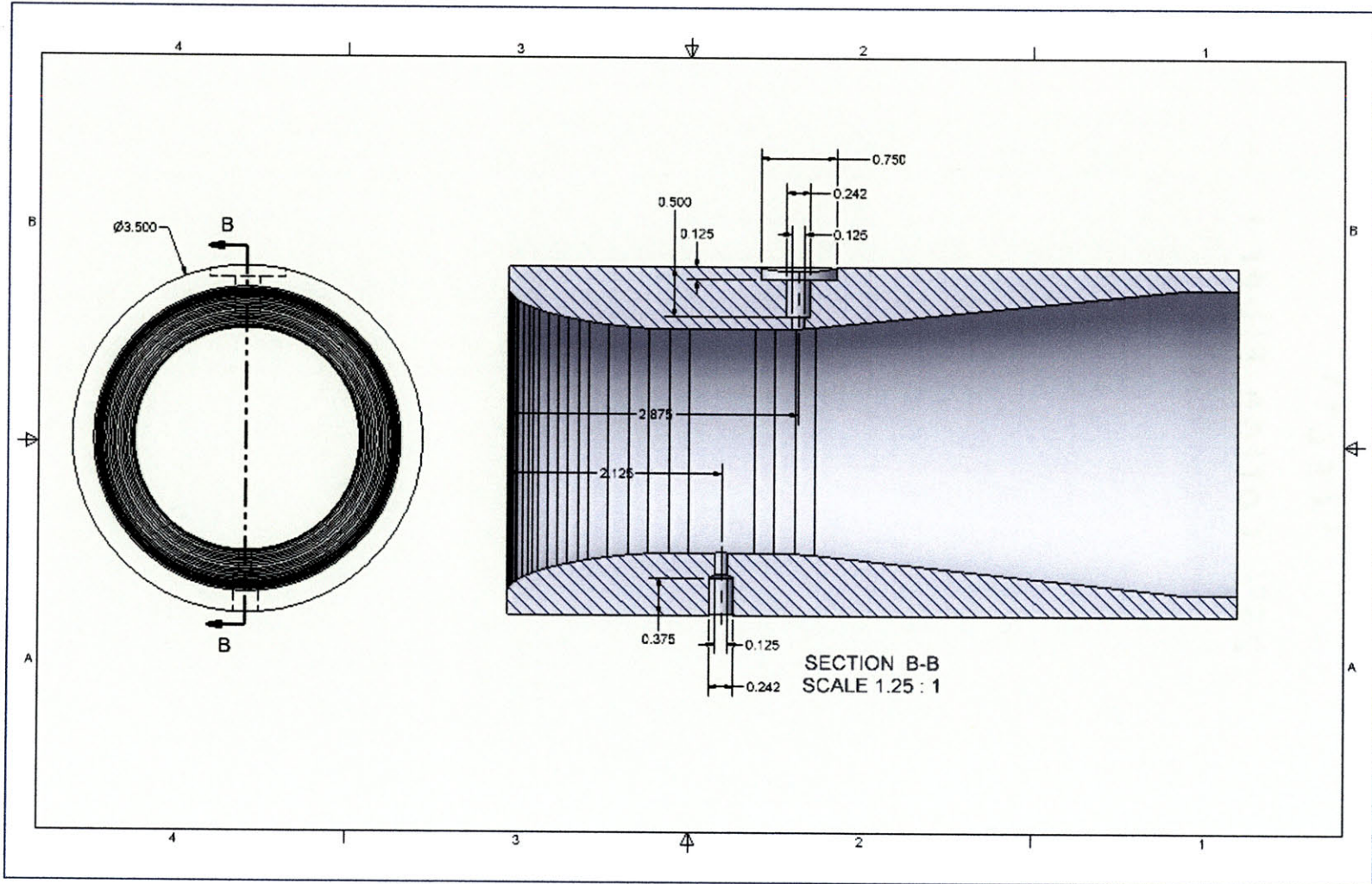| Angle	Baseline	Steady	1Hz	5Hz	10Hz
150	133.8987	133.7162	134.2057	134.4708	133.9483
145	135.4303	134.5430	135.2646	135.6812	134.6095
140	136.6198	134.9123	136.1414	136.2208	135.6413
135	138.4870	135.2336	137.0360	136.4205	136.0539
130	138.8853	135.3410	137.0722	136.3386	136.2829
125	137.8699	134.7744	136.0143	135.6106	135.6521
120	134.3427	132.5772	133.4354	132.9881	133.2771
115	129.8497	129.6133	130.5731	129.5703	129.8078
110	127.8683	126.7217	127.8233	127.1814	127.2921
100	124.5211	122.7037	124.4823	124.2176	123.9042
90	121.9042	121.8343	122.5979	122.3535	121.6447
80	119.9313	120.1107	121.3550	121.1690	120.0754

APPENDIX B

Fuel Injector Flow Rates

Water Mass Flow Rates Through Each Injector (g/s)

	400 psi 50% Duty Cycle	800 psi 50% Duty Cycle	800 psi 75% Duty Cycle
Steady	14.367	24.833	24.833
1Hz	6.8000	9.5333	12.833
5Hz	6.7333	9.4667	13.067
10Hz	6.7333	9.4333	13.400

APPENDIX C

Engineering Drawings

Ø3.500

B
B

0.750
0.500
0.242
0.125
0.125
2.875
2.125
0.375
0.125
0.242

SECTION B-B
SCALE 1.25 : 1

Venturi

95

90°

Ø0.031
Ø0.077
Ø0.156
Ø0.238
Ø0.295

A
A

0.025
0.075
0.060
90°
Ø0.016 ⍓ 0.120
0.020

SECTION A-A
SCALE 9 : 1
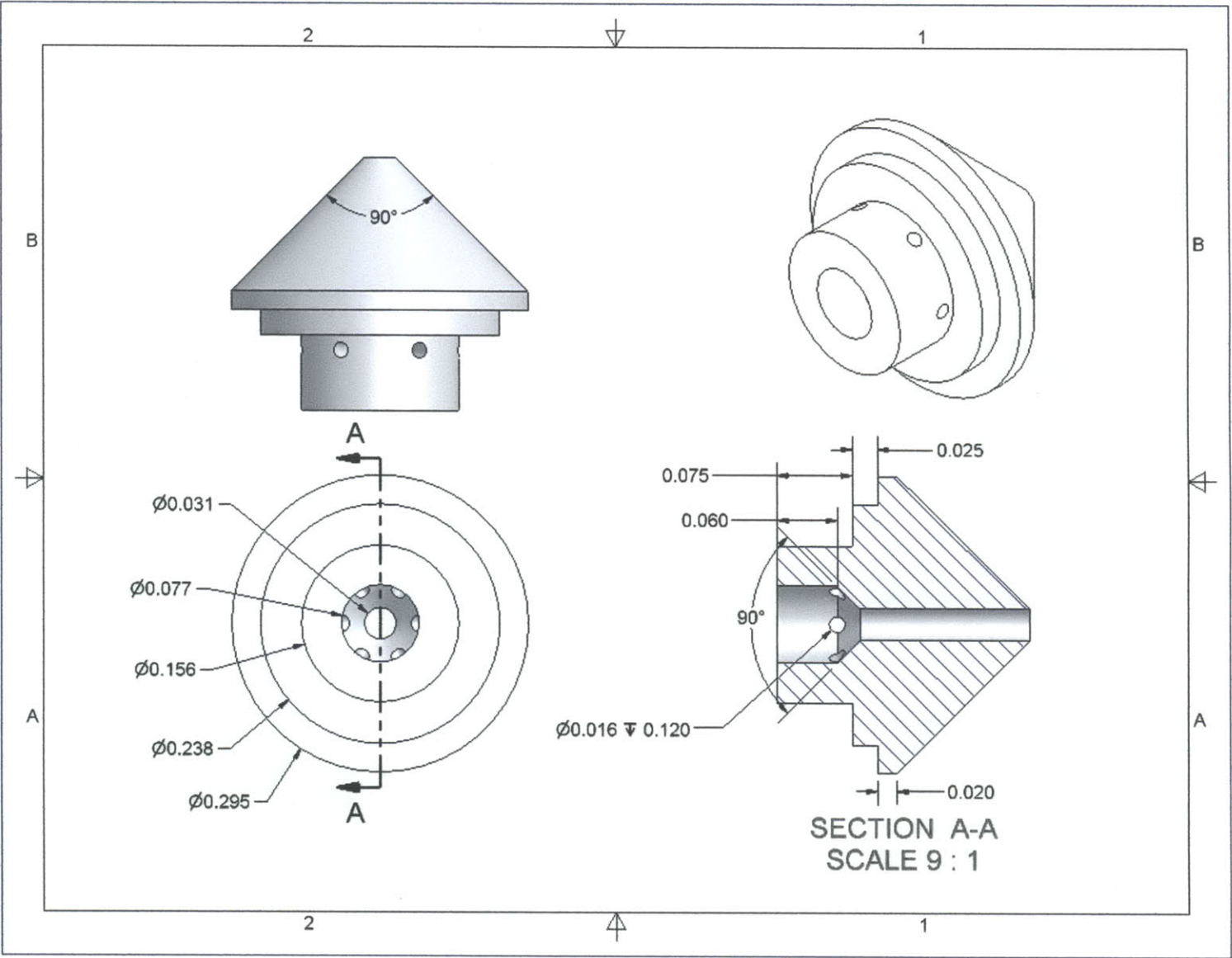
BIBLIOGRAPHY

[1] D. Papamoschou and A. Roshko. The compressible turbulent shear layer: an experimental study. *Journal of Fluid Mechanics*, 197:453-477, 1988.

[2] S. C. Crow and F. H. Champagne. Orderly structure in jet turbulence. *Journal of Fluid Mechanics*, 48:547-591, 1971.

[3] C. J. Moore. The role of shear-layer instability waves in jet exhaust noise. *Journal of Fluid Mechanics*, 80:321-367, 1977.

[4] K. A. Bishop, J.E. Ffowcs Williams and W. Smith. On the noise sources of the unsuppressed high-speed jet. *Journal of Fluid Mechanics*, 50:21-31, 1971.

[5] A. Powell. The noise of choked jets. *Journal of the Acoustical Society of America*, 25:385-389, 1953.

[6] M. B. Alkislar. Flow field measurements in a screeching rectangular jet. PhD thesis, Florida State University, 2001.

[7] L. J. S. Bradbury and A. H. Khadem. The distortion of a jet by tabs. *Journal of Fluid Mechanics*, 70:801-813, 1975.

[8] M. Samimy, K. B. M. Q. Zaman and M. F. Reeder. Effect of tabs on the flow and noise field of an axisymmetric jet. *AIAA Journal*, 31(4):609-619, 1993.

[9] D. Papamoschou and M. Debiasi. Directional suppression of noise from a high-speed jet. *AIAA Journal*, 39(3):380-387, 2001.

[10] D. Papamoschou. Noise suppression in moderate-speed multistream jets. 8th AIAA/CEAS Aeroacoustics Conference, (2002-2557), 2002.

[11] G. Raman, V. Kibens, A. Cain and J. Lepicovsky. Advanced actuator concepts for active aeroacoustic control. AIAA Paper 2000-1930, 2000.

[12] B. J. Greska. Supersonic jet noise and its reduction using microjet injection. PhD thesis, Florida State University, 2005.

[13] M. B. Alkislar, A. Krothapalli and G. W. Butler. The effect of streamwise vortices on the aeroacoustics of a Mach 0.9 jet. *Journal of Fluid Mechanics*, 578:139-169, 2007.

[14] J. S. Bendat and A. G. Piersol. *Random Data: Analysis and Measurement Procedures*. John Wiley & Sons, Inc., New York, third edition, 2000.